

# ENERGY REDUCTION IN MECHANICAL PULPING

NOVEMBER 2024



THE UNIVERSITY OF BRITISH COLUMBIA

# WELCOME MESSAGE

Dear partners in the Energy Reduction in Mechanical Pulping research program,



As Phase 3 of the program comes to a close, we want to take a moment to reflect on our achievements over the past four years. We began this phase in the midst of the COVID-19 pandemic, navigating numerous challenges and discovering new opportunities along the way. Thanks to our quick adaptation, we were able to shift our approach and stay on course.

Throughout this phase, we held a total of 9 Steering Committee meetings, both virtual and in-person, to accommodate those unable to travel. This hybrid format has significantly improved communication and increased your participation in the program. Additionally, we hosted over 100 online meetings to share results, discuss the program's direction, and incorporate your valuable feedback.

Over the years, we have had the privilege of working with 14 postdoctoral fellows, 9 graduate students (4 MAsC and 5 PhD), 5 research staff members—including management and research technicians—and 25 undergraduate students. These individuals have truly been the face of the program, and we want to express our deepest gratitude to each of them for their dedication and contributions to our success. You can find their names and faces in the final pages of this newsletter.

For the final research report of Phase 3, we encourage you to read the following pages, where we highlight the most recent work from our students and postdocs.

Looking ahead to Phase 4, we are incredibly grateful for your continued support and excited to work together for another five years, starting in 2025. The Mechanical Pulping Industry is entering a new era with fresh challenges and opportunities. We firmly believe that by collaborating, we can create a research phase focused on innovation and sustainability.

Sincerely,

A handwritten signature in black ink that reads "Mark Martinez". The signature is written in a cursive, slightly slanted style.

Mark Martinez, Ph.D., P. Eng.,  
Professor of Chemical and Biological Engineering, UBC  
Principal Investigator, ERMP Research Program



## CONTRIBUTORS

Matthias Aigner  
 Sneha Balaji  
 Rodger Beatson  
 Samuel Brown  
 Yankai Cao  
 Emily Cranston  
 James Drummond  
 Matheus Ferreira  
 Mariana Frias de Albuquerque  
 Bhushan Gopaluni  
 Siddharth Groove  
 Mark Martinez  
 Lewis Mason  
 Gloria Noki  
 Kudzanai Nyamayaro  
 James Olson  
 André Phillion  
 Scott Rennekar  
 Norman Roberts  
 Kam Russell  
 Laurel Schafer  
 Boris Stoeber  
 Heather Trajano  
 Daniela Vargas Figueroa  
 Anderson Veiga  
 Yimin Wang  
 Peter Wild  
 Adam Wu  
 Fariba Yeganeh  
 Cameron Zheng

DESIGNER CONTACT  
 Program Manager  
 Daniela Vargas Figueroa  
 daniela.figueroa@ubc.ca  
 604-827-2390

UBC Pulp and Paper Centre  
 2385 East Mall Vancouver, BC V6T 1Z4

# CONTENTS

## RESEARCH UPDATES

### System design, Sensors and Control

- 4 **PROJECT 1.1** - LC refining of mechanical pulp.
- 8 **PROJECT 1.2** - Data-driven control and analytics in the pulp and paper industry.
- 11 **PROJECT 1.3** - Creating low-energy shive-free pulps.

### Valorization of TMP fines

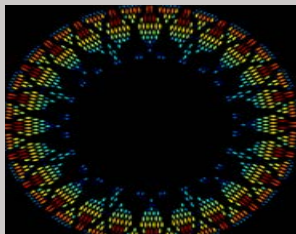
- 15 **PROJECT 2.1** - Lignin-rich fines: Simple routes towards creation of hydrophobic and hydrophilic filler additives.
- 19 **PROJECT 2.2** - From trees to treatment: Functionalizing TMP extractives.
- 24 **PROJECT 2.3** - Production, characterization, and applications of MFC derived from mechanical pulp fines.
- 29 **PROJECT 2.3B** - Incorporating microfibrillated cellulose for high strength and high bulk

### New Product Development

- 32 **PROJECT 3.1** - Chemical modification and advanced characterization of fibres
- 33 **PROJECT 3.2** - Advanced characterization - X-ray computed tomography

## PROGRAM UPDATES

- 36 **ERMP phase 3 team**
- 39 **Sharing our research**



## ON THE COVER

*Bar interaction image for a curved refiner segment provided by Valmet illustrating the distribution of energy demands across different radial positions. Author: Matthias Aigner.*

# PROJECT 1.1

## LC REFINING OF MECHANICAL PULP

Authors: Matthias Aigner, Samira Gharehkhani, Mark Martinez, James Olson, Peter Wild

### Background

Recent research from the University of Victoria has focused on refining technology using a custom piezo-ceramic force sensor to measure shear and normal forces on refiner bars. Originally tested in high consistency (HC) and low consistency (LC) refiners [Olender et al. 2008; Harirforoush et al. 2018], this sensor has proven valuable in further trials at the Pulp and Paper Centre at UBC and Catalyst Paper Excellence mill in Crofton, BC. These studies, [Aigner et al. 2020; 2022], explored the effects of operational variables on the radial distribution of forces on refiner bars. New questions have emerged about how segment geometry influences the refining process, particularly the role of parameters like bar width and bar edge length (BEL) on energy usage in LC refining.

Since then a new image-based method to quantify key refiner segment geometry parameters has been introduced, adapted from the work of Elahimehr et al. [Elahimehr et al. 2015]. Using this method, the overlap pattern between the stator and rotor bars can be examined and parameters like the size and radial position of each overlap element, as well as the number and edge length of these elements can be derived. Combining some of these refiner segment parameters with force sensor data, a method was introduced to estimate power expenditure for each overlap element and for the refiner as a whole using data from the baseline study conducted previously [Aigner et al. 2024].

In this edition of the newsletter, the authors delve into recent insights regarding the trends observed in overlap patterns between the stator and rotor bars. Understanding these patterns is crucial, as they directly influence the efficiency and effectiveness of the refining process. The authors also discuss

progress in the power prediction model, which now integrates additional data from a different trial to provide a more accurate estimate of power expenditure across different operational conditions. By expanding the model, the goal is to enable better predictions of power usage, based on segment geometry

### Results

#### *Trends in Segment Interaction Pattern*

To investigate trends in segment interaction patterns, the refiner segments used in the baseline study [Aigner et al. 2024] were analyzed using the image-based analysis tool. This tool enables a detailed examination of segment geometry and the interaction patterns between the stator and rotor bars. To expand upon these findings and compare the performance of different segment types, a refiner segment from an earlier study [Aigner et al. 2020] was also included. Table 1 provides the specifications for all segments analyzed, including segments P1, P2, and P3 from the baseline study, as well as segment A1 from previous work.

The primary difference in geometry between these segments lies in bar shape: P1, P2, and P3 feature curved bars, whereas A1 is designed with straight bars. This distinction in bar design is expected to influence the refining dynamics, as the shape and orientation of the bars directly impact the bar interaction.

The operating conditions for each trial are also listed in Table 1. Notably, the trial using segment A1 was a tank-to-tank run, meaning that the pulp passed through the refiner only once. In contrast, the trials with segments P1, P2, and P3 were conducted in a recirculation setup, where the pulp was cycled through the refiner multiple times, accumulating energy put on the fibres. This difference in trial setup allows for a broader comparison of segment performance under varying refining conditions.

**Table 1.** Refiner segment specifications

	P1	P2	P3	A1
Bar type	curved	curved	curved	straight
BEL [km/rev]	2.1	5.4	2.1	2.74
Bar width [mm]	1.4	1.4	2.5	1.6
Groove width	3.8	1.9	2.7	3.2
Trial Information				
Fiber length [mm]	1.45			1.9
Trial type	recirculation			tank to tank
Rotational speed [rpm]	1200, 1600			1400
Consistency (%)	3.5			
Flow [l/min]	250 [l/min]			

To compare the interaction patterns of curved and straight bars, segments P1 and A1 were selected. These segments are closely matched in terms of key geometric parameters, with bar widths of 1.4 mm for P1 and 1.6 mm for A1, and similar bar edge lengths (BEL) of 2.1 km/rev and 2.74 km/rev, respectively. By focusing on these segments, the analysis aims to isolate the effect of bar shape on refining behaviour, particularly in terms of segment interaction patterns and refining efficiency.

The bar interaction pattern for segment P1 is illustrated in Figure 1. The area and radial position of each overlap element is shown in Figure 1(a). The overlap elements follow an exponential progression, with the curvature of the bars creating a more pronounced overlap near the periphery, resulting in larger overlap areas in that region. Moving radially outward along the bars, the overlap elements' size increases continuously, forming

a non-linear, exponential relationship between area and radial position. Clusters of overlap elements also shift outward in this radial position plot, forming a curved orientation. One prominent cluster spans from an area of 3 to 10 mm<sup>2</sup> and extends from a radial position of 0.13 to 0.18 m.

The bar interaction pattern for segment A1, displayed in Figure 2, exhibits distinct characteristics compared to P1. Like P1, the area and radial position of each overlap element are shown in Figure 2(a). However, in A1, the overlap elements progress along a more linear path, reflecting the straight bar design of this segment. The overlap clusters here create "shelves" that move outward radially and increase in size, forming a stepped staircase-like pattern. One notable cluster is visible between 0.15 and 0.19 m in radial position, with an area size of approximately 9 mm<sup>2</sup>.

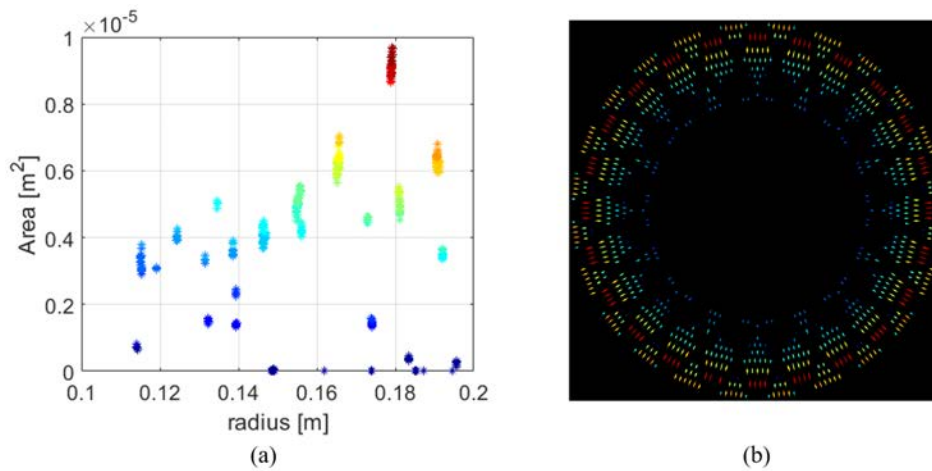


**Figure 1.** Scatter plot (a) and bar interaction image (b) for refiner segment P1. The scatter plot shows the radial location of overlap areas and their respective sizes. The bar interaction image shows the location of the overlap areas around the refiner segment. The colour-coding is done based on the power factor which is the product of area and radial distance. Highest in dark red, and lowest in dark blue.

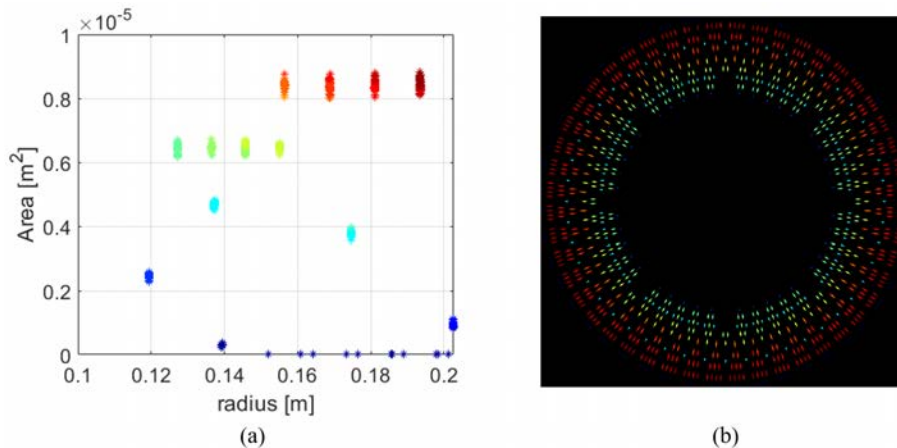


**Figure 2.** Scatter plot (a) and bar interaction image (b) for refiner segment A1. The scatter plot shows the radial location of overlap areas and their respective sizes. The bar interaction image shows the location of the overlap areas around the refiner segment. The colour-coding is done based on the power factor which is the product of area and radial distance. Highest in dark red, and lowest in dark blue.

# PROJECT 1.1

In a previous newsletter a power estimation tool was introduced [Aigner et.al. 2024]. This tool is based on the assumption that the gross power required by the refiner can be estimated using the size of each individual overlap element,  $A_i$ , its radial position  $r_i$ , the rotational speed  $\omega$ , and the tangential shear stress  $\tau$ . Together, these variables are combined in the following equation:

$$P = \sum_{i=1}^{N_c} P_i = \sum_{i=1}^{N_c} \tau A_i r_i \omega \quad (1)$$

where  $P$  is the total expended power for the refiner,  $P_i$  is the power expended over an individual overlap element  $i$ , and  $N_c$  is the total number of overlap elements. At this point, the model assumes that shear stress is constant.

Using Equation 1, the contribution of each individual overlap element to the total power can be calculated based purely on segment geometry, resulting in a derived expression for the “geometry factor”:

$$I = \sum_{i=1}^{N_c} I_i = \sum_{i=1}^{N_c} A_i r_i \quad (2)$$

Here  $I$  represents the total “geometry factor” for a refiner segment, while  $I_i$  denotes the individual “geometry factor” for an overlap element  $i$ . This geometry factor enables the visualization of overlap patterns, highlighting how individual elements contribute to power consumption based on their position. Figures 1(b) and 2(b) display these visualizations for segments P1 and A1, respectively. In each figure, the overlap elements are colour-coded by their geometry factor: red indicates a high-power factor, while blue signifies a low power factor, effectively illustrating the distribution of energy demands across different radial positions.

The geometry factor underscores that, under a constant shear stress assumption, overlap elements farther from the center experience a higher power factor than those closer to the center, even if both elements are identical in size. This model enables a more nuanced comparison of refiner segments by visualizing differences in energy distribution across the refiner.

In summary, although both refiner segments reach comparable overlap area sizes at the periphery, the progression of overlap elements along the radial path differs significantly. Segment A1, with its staircase-like pattern, shows an oscillating geometry factor due to the sequential, shelf-like formation of overlap clusters. In contrast, segment P1 displays a smoother, continuous

progression of overlap elements, leading to a more stable and evenly distributed power factor. These contrasting overlap patterns reflect the influence of bar shape on energy distribution, with A1's straight bars creating discrete steps in power consumption, while P1's curved bars yield a more consistent power distribution across the radial span.

## *Power Estimation Expanded*

The previously developed power estimation tool was applied to data for trials run with segment A1. This expanded use of the power estimation tool has proven valuable in demonstrating the tool's versatility and reliability across different refiner segments and refining conditions. By allowing direct comparisons between segments P1, P2, and P3, as well as the newly tested A1, the tool has shown strong adaptability and accuracy in predicting power consumption under various conditions. This adaptability is particularly important as a first step towards a robust way to estimate power consumption consistently and reliably.

The results, shown in Figure 3, illustrate the tool's robust performance across a broad power range. Segment A1, which operates from below 20 kW to above 90 kW, provides an ideal test case for assessing the tool's effectiveness under different operational conditions. This addition expands the range of scenarios tested, validating the tool's utility for segments with diverse power demands. Data from previous trials with P1, P2, and P3 has served as a baseline, allowing a detailed comparison and reinforcing the tool's accuracy at lower power levels.

However, Figure 3 also reveals a limitation in the tool's predictive capacity at higher power levels. While the calculated power for A1 plateaus around 50 kW, the measured power continues to rise, highlighting a discrepancy that suggests the tool may need further refinement for accurate predictions beyond this threshold. This plateau points to a potential gap between the tool's model assumptions and the physical reality at higher power conditions.

The addition of segment A1 underscores the importance of ongoing validation and refinement to extend the tool's accuracy to encompass higher power levels. Despite this limitation, the power estimation tool remains highly valuable for power levels below 50 kW, and current investigations into the observed discrepancy are aimed at identifying factors that could improve its applicability across an even wider range of refining scenarios.

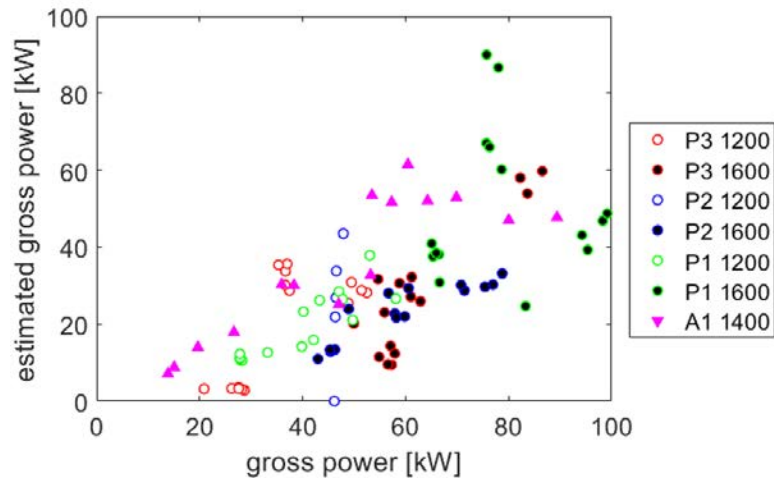


**Figure 3.** Calculated gross power plotted against measured gross power. Calculated power is derived based on novel segment geometry parameters and force measurements. Data in this figure includes data collected in recent trials at the PPC as well as trials from previous work done at the PPC with a different refiner segment as well as different pulp furnishes.

## Future Research

To investigate the impact of bar width on refining performance, a new series of trials was designed. Specifically, these trials aim to compare segments with narrow bar widths against those with wider bar widths, using paired combinations in which each narrow-bar segment is matched with a wide-bar segment, and vice versa. The goal is to observe differences in refining behaviour, force profiles, and loadability across these configurations. Since these trials use the same refiner segments from the previous baseline study [Aigner et.al. 2024], the findings are anticipated to build upon and enhance the value of that research, providing a more comprehensive understanding of bar width effects.

The first set of trials was successfully completed in October 2024, marking an initial step in this investigation. These trials aim to provide insights into how bar width influences refining dynamics and, thereby, contribute to refining process optimization.

## Acknowledgements

The authors thank Mr. Norm Roberts for conducting the refining trials and the co-op students at the UBC-PPC for their hard work in analysing the fibre data.

## References

1. Aigner, M., Olson, J., and Wild, P. (2020). Measurement and interpretation of spatially registered bar-forces in LC refining. *Nordic Pulp & Paper Research Journal*, 35(4), 600-610.
2. Aigner, M., Olson, J., Sun, Y., and Wild, P. (2022). Interpretation of force profiles in mill-scale LC refining. *Nordic Pulp & Paper Research Journal*, 37(1), 42-53.
3. Aigner, M., Gharekhani, S., Martinez, M., Olson, J., and Wild, P. (2023). Project 1.1: LC Refining of Mechanical Pulp. Energy reduction in mechanical pulping – November 2023- Newsletter, p4-8.
4. Aigner M., Wild, P., Gharekhani, S., Lacourse, T., Martinez, M. Martinez, and Olson, J. (2024). A comprehensive LC-refiner study, In Proceedings for the International Mechanical Pulping Conference 2024., pp. 123–129, 2024.
5. Elahimehr, A., Olson, J. A. and Martinez, D. M. (2015): Low consistency refining of mechanical pulp: how plate pattern and refiner operating conditions change the final properties of pulp, *Nord. Pulp Pap. Res. J.*, 30(4), 609–616.
6. Aigner, M., Martinez, M., Olson, J., and Wild, P. (2024). Project 1.1: LC Refining of Mechanical Pulp. Energy reduction in mechanical pulping – June 2024- Newsletter, p4-8.
7. Harirforoush, R, Olson, J., and Wild, P. (2018). In-Process Detection of Fiber Cutting in Low Consistency Refining Based on Measurement of Forces on Refiner Bars. *Tappi Journal* 16 (4): 460–69.
8. Olender, D., Wild, P., & Byrnes, P. (2008). A piezoelectric force sensor for mill-scale chip refiners. *Proceedings of the Institution of Mechanical Engineers, Part E: Journal of Process Mechanical Engineering*, 222(2), 115-122.

# PROJECT 1.2

## DATA-DRIVEN CONTROL AND ANALYTICS IN THE PULP AND PAPER INDUSTRY

Authors: Siddharth Grover, Bhushan Gopaluni, Yankai Cao

### Background

Mechanical pulping, a process that converts lignocellulosic materials into pulp through the application of mechanical energy without the use of chemicals, remains a cornerstone of pulp production. In the context of modern manufacturing, this process is increasingly data-driven, reflecting the growing complexity and sophistication of industrial operations. Historically, the focus has been on maximizing output and efficiency while minimizing downtime and production delays (Yin et al., 2023). However, the recent emphasis on sustainability has introduced new challenges and priorities, adding complexity to efforts aimed at process optimization.

Paper manufacturing machinery is often equipped with one or more sensors to capture trends in equipment behaviour, and machine health, and make inferences about remaining useful life. However, manufacturing systems are quite complex because they often require human intervention, and deal with equipment failure and inefficiencies - which makes them unpredictable. Existing models, such as ETS, EWMA, ARIMAX, and SARIMAX rely on the assumptions of stationarity, invertibility, and statistically insignificant residual correlation. Stationarity is the idea that statistical properties of a process, such as mean, variance and autocorrelation remain constant over time. Invertibility implies that a process is an infinite autoregression - a process  $X_t$  is invertible if and only if

$$X_t = \sum_{j=1}^{\infty} a_j X_{t-j} + w_t$$

with the restriction that

$$\sum_{j=1}^{\infty} a_j^2 < \infty$$

Many of these assumptions are difficult to satisfy, even after transformations (such as Box-Cox), de-trending, and removing seasonality. As a result, identifying anomalies based on mathematical models becomes challenging - especially for the pulp and paper manufacturing industry, which requires manual intervention many times.

In earlier works, Rewicki et al. showed the advantage of AutoEncoders over other deep learning methods by comparing three classic machine learning methods and three deep learning-based methods for anomaly detection on time series. They concluded that, depending on the type of anomaly and computing time, classical approaches could be outperformed with deep anomaly detection. AutoEncoders are trained on normal data which is compressed and reconstructed - instances that cannot be reconstructed well (or have a high anomaly score) are considered anomalies. Forecasting-based methods take in current and previous time-series data to make predictions for the future, with the difference between actual and predicted values serving as an anomaly score. Generative models such as Generative Adversarial Networks (GANs) and Variational AutoEncoders (VAEs) also exist. GANs train two networks - a generator that creates synthetic and real data to fool the discriminator, and a discriminator to identify synthetic data from real data.

To address the limitation of classical methods, we propose a cutting-edge, assumption-free neural architecture: a (Long Short Term Memory) LSTM encoder-decoder model. This model reconstructs “normal” operational patterns from training data and identifies anomalies by measuring reconstruction errors. The figure below shows the structure of an LSTM encoder-decoder model:

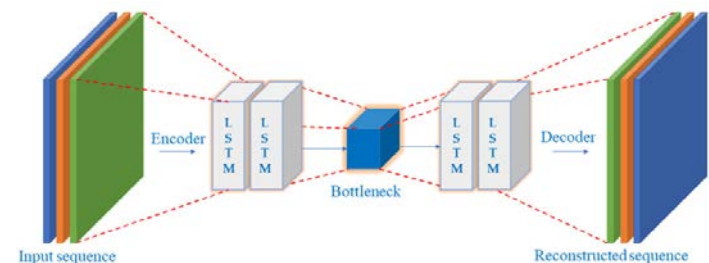


Figure 1. LSTM Encoder-Decoder

# PROJECT 1.2

Unlike traditional statistical models, the LSTM-based approach adapts to dynamic, high-dimensional data without relying on assumptions about the underlying process. Furthermore, it excels in capturing temporal dependencies and contextual variations, making it ideal for complex and data-rich environments like pulp manufacturing. The performance of this LSTM encoder-decoder is compared to both classical and deep learning methods for anomaly detection. The proposed LSTM encoder-decoder model introduces several key improvements to the landscape of anomaly detection within the pulp and paper industry:

- *Assumption-Free Framework:* By eliminating reliance on stationarity, invertibility, or low residual correlation, the model overcomes the limitations of traditional methods that struggle with non-linear, high-dimensional, and evolving datasets.
- *Dynamic Adaptability:* The model's sequence-learning capability allows it to adapt to temporal dependencies and contextual variations in data, ensuring robustness even in dynamic production environments with frequent human intervention.
- *Enhanced Detection Accuracy:* By reconstructing normal operational patterns and using reconstruction error as a metric for anomaly detection, the model is capable of identifying both subtle and extreme anomalies, reducing false positives and improving precision.
- *Scalability Across Complex Systems:* The neural network architecture can handle high-dimensional sensor data and learn patterns across multiple operational units, making it ideal for complex systems like those in pulp and paper manufacturing.
- *Reduction in Manual Intervention:* Unlike conventional methods that require preprocessing steps such as detrending and seasonal adjustment, the LSTM model operates on raw data, significantly reducing the need for human oversight and simplifying the deployment pipeline.

## Proposed Methodology & Progress Summary

### *Benchmarking on the TEP Dataset*

TEP is based on an existing plant and the processes running in it. The data itself is synthetic, i.e., a simulation of the plant. It consists of five main modules, each a two-stage reactor, a condenser, a vapour-liquid separator, a stripper, and a reboiler, as well as 11 pneumatic valves, two pumps, and a compressor. TEP has been used extensively for anomaly detection tasks for the last

30 years (Downs & Vogel, 1993). This dataset contains synthetic data from 20 different erroneous runs and 1 error-free run, with 53 parameters.

### *Models*

Many model types, such as those involving Generative Adversarial Networks (GANs), Forecasting (LSTMs), Reconstruction (AutoEncoders), and hybrid models are tested. Some of these include the OmniAnomaly, USAD, GenAD and many more.

### *Metrics*

To compare the performance of different algorithms with each other, one or more metrics need to be devised. An anomaly detection algorithm works by generating an anomaly detection score, with scores beyond a certain threshold indicating an anomaly. To compare the anomaly detection performance of different models, a variety of metrics may be used.

- *F-score is a measure of predictive performance.* It is calculated from the precision and recall of the test, where the precision is the number of true positive results divided by the number of all samples predicted to be positive, and the recall is the number of true positive results divided by the number of all samples that should have been identified as positive.
- *Area Under The Precision-Recall Curve (AUPRC)* is a metric used to evaluate the performance of classification models by summarizing the information in a precision-recall (PR) curve. AUPRC measures the area under the PR curve, which plots precision on the y-axis and recall on the x-axis. Both precision and recall are values between 0 and 1. AUPRC is often used in situations with imbalanced classes, though it is not ideal for situations where false negatives are costly. In those cases, an Area Under The Receiver-Operator Curve (AUROC) is used. AUROC is a performance measurement that summarizes the Receiver Operating Characteristic (ROC) curve into a single number. The ROC curve plots the True Positive Rate (TPR) against the False Positive Rate (FPR). Since the cost of false negatives (undetected anomalies) is higher than the cost of other predictions, an AUROC may be a better measure for AD than an AUPRC.

### *Evaluation and Implementation*

For robust and comparable results, all the models will be implemented in PyTorch and 5-fold cross-validation will be used. Once the models are prepared, they will be tested on the TEP dataset and then the private dataset.

# PROJECT 1.2

## Conclusion and Future Work

This study addresses a critical need for robust anomaly detection in the pulp and paper industry by leveraging a novel LSTM encoder-decoder model. By eliminating the limitations of traditional statistical methods, the proposed model provides a dynamic, assumption-free framework capable of identifying anomalies in real time across complex manufacturing environments. Benchmarking against the TEP dataset demonstrated the model's superior detection accuracy, adaptability, and scalability when compared to classical and contemporary deep learning approaches.

- *Integrating Causal Bayesian Networks (CBNs)*: to complement the LSTM model, integrating causal Bayesian networks can provide insights into the underlying relationships between operational parameters. Structure learning with CBNs has been demonstrated in works like Glymour et al. (2019) to enhance interpretability and facilitate root cause analysis of anomalies. This integration would enable a holistic approach to anomaly detection and process optimization.
- *Exploration of One-Class Classification for Time Series Anomaly Detection*: Inspired by the success of supervised classifiers, one promising avenue is to explore "one-class classification" methods for anomaly detection. These techniques involve training a network to map normal samples to a hypersphere or hyperplane while separating anomalous data (Schölkopf et al., 2001; Ruff et al., 2018). Recent works have extended this paradigm to time-series anomaly detection, achieving promising results by leveraging temporal dependencies (Zong et al., 2018; Chalapathy et al., 2019).

## References

1. Downs, J. J., and Vogel, E. F. "A Plant-Wide Industrial Process Control Problem." *Computers & Chemical Engineering*, vol. 17, no. 3, 1993, pp. 245–255.
2. Glymour, et al. *Causal Inference*. MIT Press, 2019.
3. Schölkopf, Bernhard, et al. "Estimating the Support of a High-Dimensional Distribution." *Neural Computation*, vol. 13, no. 7, 2001, pp. 1443–1471.
4. Ruff, Lukas, et al. "Deep One-Class Classification." *Proceedings of the International Conference on Machine Learning (ICML)*, 2018.
5. Chalapathy, Raghavendra, et al. "Anomaly Detection Using One-Class Neural Networks." *IEEE Transactions on Knowledge and Data Engineering*, vol. 32, no. 3, 2019, pp. 568–576.
6. Yin, Zhiyong, et al. "Anomaly Detection in Time Series with Machine Learning: A Review and Prospects." *Chemical Engineering Research and Design*, 2023.
7. Rewicki, Dominik, et al. "Deep Learning for Industrial Time Series Anomaly Detection: Benchmarking and Evaluation." *Computers in Industry*, 2022
8. Mobarakeh, Maedeh Rahnama, et al. "Pulp and Paper Industry: Decarbonisation Technology Assessment to Reach CO2 Neutral Emissions—An Austrian Case Study." *Energies*, vol. 14, no. 4, 2021, pp. 1161–1185

## CREATING LOW-ENERGY SHIVE-FREE PULPS

Authors: Rodger Beatson, Heather Trajano, Gloria Noki

### Background

The objectives of this project are to: (1) generate understanding of the impact chemical treatments have on the development of fibre and fines' properties during LC refining, and (2) develop economically viable low energy processes that combine such treatments with LC refining to produce printing/writing, board and packaging grades.

Previous work by Chang et al. (2016) compared the effects of alkaline peroxide, chlorine dioxide, and ozone treatments with subsequent LC refining on TMP. Results showed that introducing oxidative agents reduces electrical energy consumption and improves pulp strength. Alkaline peroxide is hypothesized to generate acid groups on the surface of fibres and fines, increasing surface charge and causing surface fibre swelling. Swelling increases the bonded surface area and causes sheet densification. Chlorine dioxide and ozone are also thought to oxidize lignin to produce carboxylic acids. A subsequent alkali soak forms sodium salt, which brings about softening and swelling of fibres and fines, leading to increase in tensile strength.

Previous investigations of Highly Alkaline Peroxide Treatment (HAPT) have been conducted by varying the concentration of hydroxide ions (pH), concentration of hydrogen peroxide, temperature and treatment time. The current approach to advance HAPT includes studying the effect of fibre length and coarseness on tensile strength, acid group generation and other property developments of handsheets.

### Materials and Methods

#### Pulp Characterization

The secondary refiner TMP was provided by Holmen Braviken. 10 g OD pulp was hot disintegrated using standard procedures. The suspension was then fractionated with a Bauer McNett using standard procedures. The whole pulp was composed of 71% long fibres, which were retained in the 14, 28, 48, 100 and 200 mesh sieves. The filtrate containing fines was discarded. The pulp was characterized using a fibre quality analyzer (FQA). The relevant fibre characteristics are summarized in Table 1. Figure 1 shows the correlation between fibre length and coarseness, which is proportional to fibre wall thickness.

#### Separation of Fibres and Fines

Batches of 20 g OD pulp were hot disintegrated using standard procedures. Distilled water was added to achieve 0.5% consistency. The Bauer McNett fibre classifier was used to separate whole pulp into fractions with narrow fibre length distributions. This process was repeated until sufficient amounts of each fibre fraction were collected for subsequent testing. The filtrate containing fines was discarded.

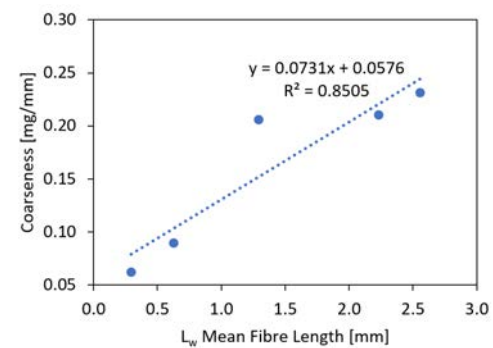


Figure 1. Coarseness as a function of fibre length.

Table 1. Pulp Characterization

Mesh	Length-weighted Mean Fibre Length		Mean Fibre Width		Coarseness		
	Sieve #	L <sub>w</sub>	σ <sub>Lw</sub>	W	σ <sub>w</sub>	C	σ <sub>c</sub>
		mm	mg/m	μm	μm	mg/m	mg/m
14		2.555	0.004	29.95	0.45	0.231	0.011
28		2.231	0.003	31.85	0.36	0.210	0.007
48		1.293	0.003	27.85	0.24	0.206	0.010
100		0.625	0.004	21.80	0.33	0.090	0.002
200		0.295	0.005	18.35	0.83	0.062	0.001
<b>Whole Pulp</b>		1.140	0.005	26.05	0.37	0.168	0.005

## Highly Alkaline Peroxide Treatment

Prior to HAPT, all fibre fractions were chelated with a 0.2% charge diethylene triamine pentaacetic acid (DTPA) at 4% consistency at 60°C in a water bath for 30 minutes. The pulp was then washed with distilled water.

The chelated pulp was treated in a plastic bag with 4% H<sub>2</sub>O<sub>2</sub>, 6% NaOH and 3% Na<sub>2</sub>SiO<sub>3</sub> at 10% consistency and 65°C for 60 minutes. Mixing was achieved by squeezing the bag every 5 minutes for the first 10 minutes, every 10 minutes for the next 20 minutes, and every 30 minutes for the remaining duration of the treatment. After treatment, the plastic bag containing treated pulp was cooled in an ice water bath.

The pulp suspension was then filtered. The final pH and residual peroxide of the HAPT filtrate were measured. Residual peroxide was determined using iodometric titration with 0.1 N sodium thiosulfate as the titrant. The pulp was then washed with distilled water. Weak acid content was determined using conductometric titration (June 2022 Newsletter).

For the controls, each fibre fraction was chelated, washed and used to prepare a 10% consistency suspension. The pulp suspension was incubated at 65°C for 60 minutes without H<sub>2</sub>O<sub>2</sub>, NaOH and Na<sub>2</sub>SiO<sub>3</sub>. The mixing protocol was applied. The final pH and weak acid content were determined.

Handsheets were prepared from the HAPT and control pulps according to TAPPI standard method T205. Handsheet properties were determined according to TAPPI standards.

## Results

### Final pH and Residual Peroxide

After treatment for 60 minutes, there was little variation in the pH with respect to fibre length for HAPT and control fibres as shown in Figure 2. The difference in final pH between HAPT and control is due to the presence and absence of sodium hydroxide, respectively.

Figure 3 shows that the residual peroxide increases as coarseness increases, indicating that peroxide consumption is faster in the shorter less coarse fibres, likely due to their higher specific surface area and thinner cell walls.

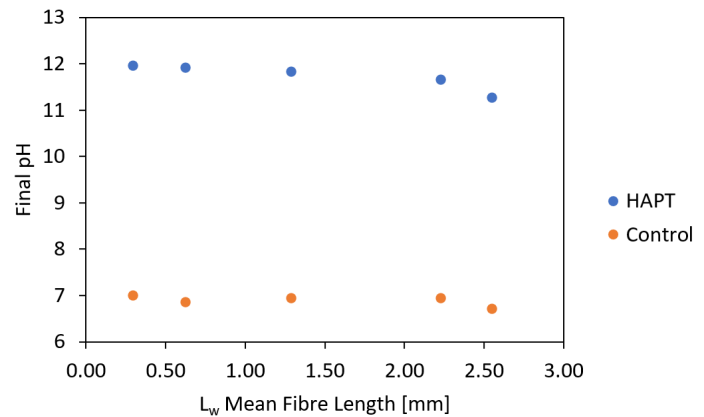


Figure 2. Final pH as a function of mean fibre length

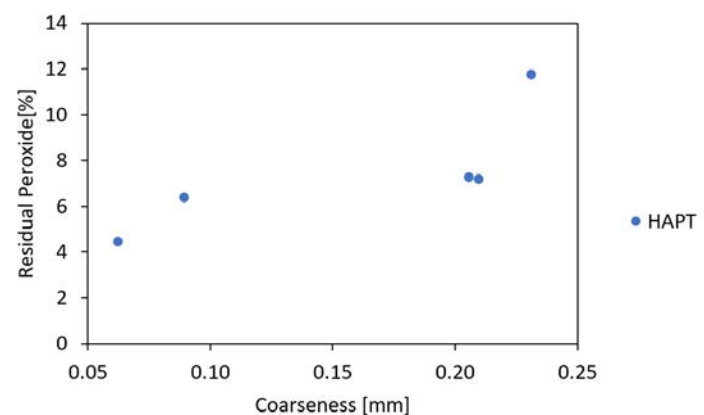


Figure 3. Percentage residual peroxide increases as coarseness increases.

### Pulp Properties

The absorption coefficient decreases as the fibre length increases, especially for the control (Figure 4). This is probably due to a higher lignin content of the finer material. The lower absorption coefficient for the HAPT pulp is a result of brightening by the hydrogen peroxide. The high scattering coefficient for the short fibre fractions is due to their higher specific surface area (Figure 5). It is interesting to note that the behaviour of both HAPT and control is similar and that brightening has little influence on the scattering coefficient. Figure 6 shows that the brightness decreases as length increases for both the control and HAPT pulps which is a result of decreasing specific surface area. The high brightness for the HAPT pulp is a result of the removal of chromophores by peroxide brightening.

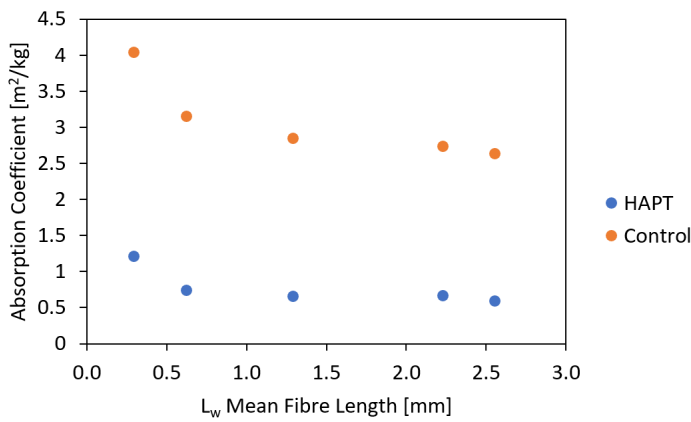


Figure 4. Absorption coefficient decreases as fibre length increases.

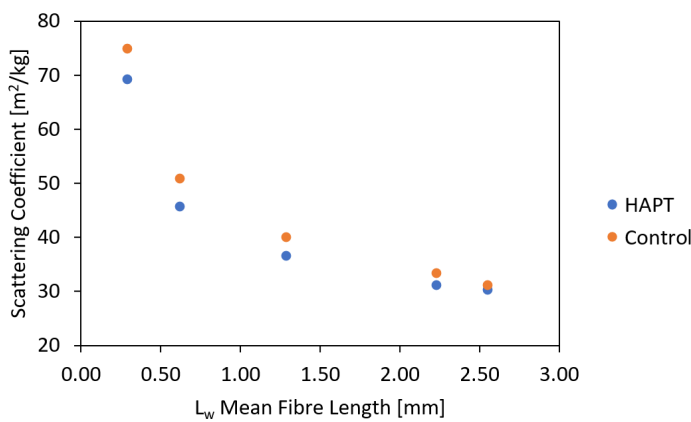


Figure 5. Scattering coefficient decreases as fibre length increases.

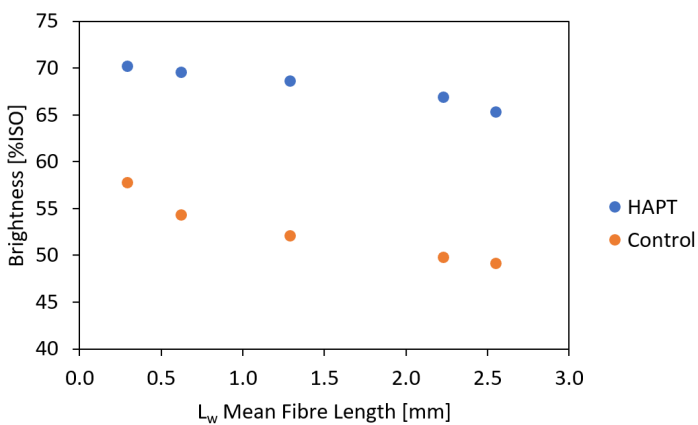


Figure 6. Brightness decreases as fibre length increases.

Figure 7 shows that the gain in tensile strength on HAPT treatment decreases as fibre length increases. The development of tensile strength is higher in the shorter less coarse fibres, possibly due to the greater extent of reaction with peroxide on account of their larger specific surface area.

The tear increases as fibre length increases for both the control and HAPT pulps (Figure 8). This reflects the high dependence of tear on fibre length. The tear resistance of HAPT pulp is higher on account of the enhanced fibre bonding.

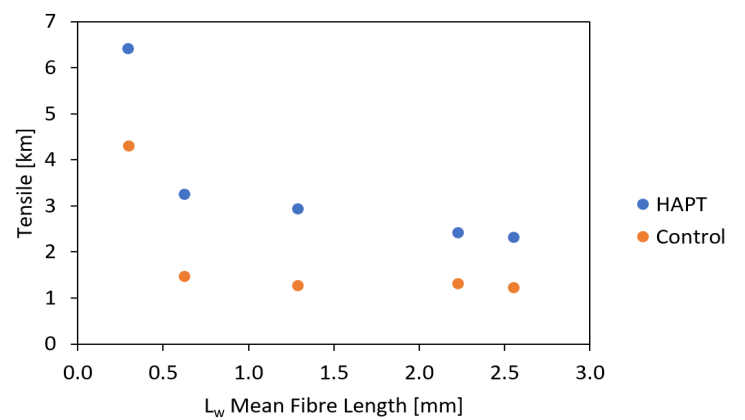


Figure 7. Tensile strength decreases as fibre length increases.

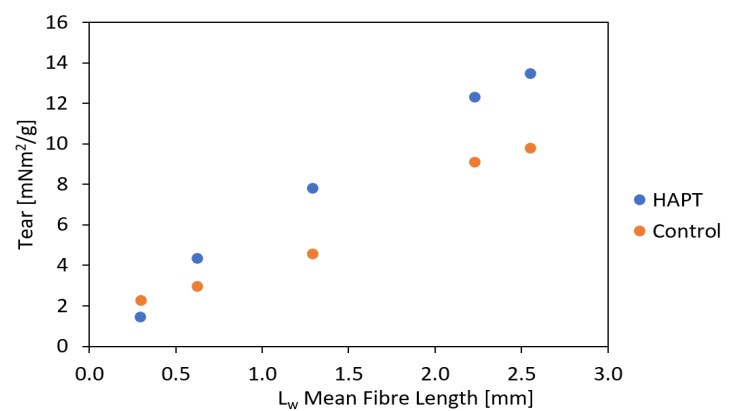


Figure 8. Tear increases as fibre length increases.

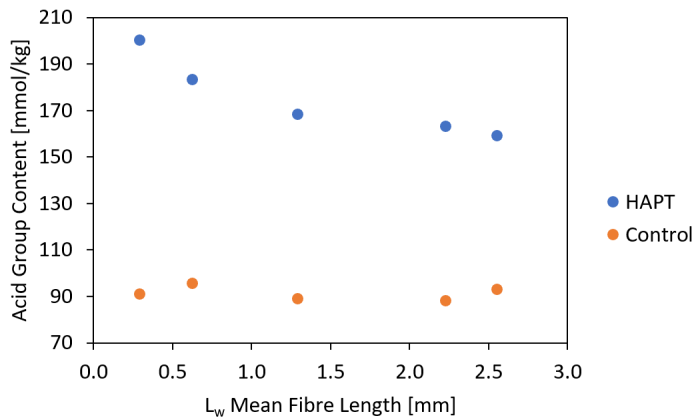


Figure 9. Acid group content as a function of fibre length

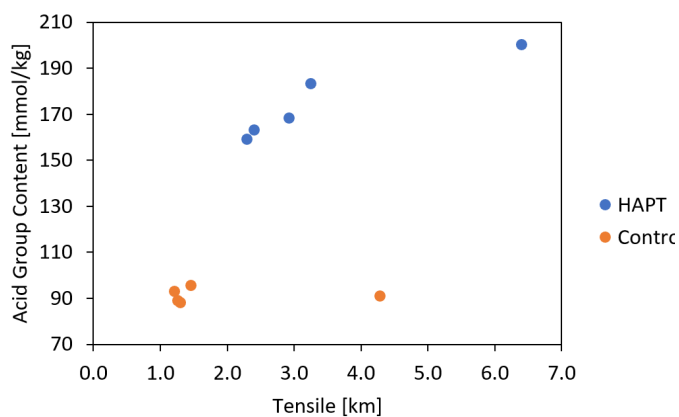


Figure 10. Acid group content as a function of fibre length

## Results (cont.)

Figure 9 shows that the quantity of acid group content initially present in each fibre fraction of the control is approximately constant. These are the carboxylic acid groups arising from the hemicelluloses. The change in acid group content after HAPT is greater in the shorter less coarse fibres, likely due to their higher lignin content resulting in higher formation of muconic groups.

Figure 10 shows that the tensile strength develops with acid group generation, further supporting the hypothesis that strength gains from HAPT are partly owing to the acid group generation.

## Conclusions

Peroxide reaction with pulp is faster in the shorter less coarse fibres as evidenced by the lower residual peroxide and higher acid group content. This is likely due to the fibres' higher specific surface area, thinner cell walls, and higher lignin content. Brightness decreases as the fibre length increases due to the decreasing specific surface area. After HAPT, tear resistance increases due to the enhanced fibre bonding. The change in of tensile strength is highest in shorter less coarse fibres due to their rapid reaction with peroxide. Acid group content and tensile strength correlate thus providing further support for the hypothesis that strength gains from HAPT are partly owing to acid group generation.

## Future Work

In future work, a detailed characterization of fines and fibres will be performed, prior to and post HAPT. Additionally, a kinetics model of the tensile strength and acid group generation will be developed.

## References

1. Beatson, R., Trajano, H., Mitra, S., K., and Maulit, C. (2021, November). ERMP November 2021 Newsletter. Energy Reduction in Mechanical Pulping. [https://ermp.sites.olt.ubc.ca/files/2022/06/ERMP\\_Nov2021.pdf](https://ermp.sites.olt.ubc.ca/files/2022/06/ERMP_Nov2021.pdf)
2. Chang, X. F., Luukkonen, A., Olson, J., & Beatson, R. (2016). Pilot-scale investigation into the effects of alkaline peroxide pre-treatments on low-consistency refining of primary refined softwood TMP. *Bioresources*, 11(1), 2030-2042. <https://doi.org/10.15376/biores.11.1.2030-2042>
3. Dence, C., W., and Omori, S., (1996). Survey of hydrogen peroxide bleaching of mechanical and (chemi)mechanical pulp - factors affecting brightness. *Pulp Bleaching: Principles and Practice: TAPPI 1996*, pp. 457-489.
4. Maulit, C., Beatson, R., Trajano, H., Po, R., and Lai, R. (2022, November). ERMP November 2022 Newsletter. Energy Reduction in Mechanical Pulping.
5. Mitra, S., K., Maulit, C., Beatson, R., and Trajano, H. (2022, June). ERMP June 2022 Newsletter. Energy Reduction in Mechanical Pulping. [https://ermp.sites.olt.ubc.ca/files/2023/01/ERMP\\_June2022.pdf](https://ermp.sites.olt.ubc.ca/files/2023/01/ERMP_June2022.pdf)
6. Moldenius, S., (1984). The Effects of Peroxide Bleaching on the Strength and Surface Properties of Mechanical Pulping. *Journal of Pulp and Paper Science.*, vol. 10, pp. 172-177.

## LIGNIN RICH FINES: SIMPLE ROUTES TOWARDS CREATION OF HYDROPHOBIC AND HYDROPHILIC FILLER ADDITIVES

Authors: Adam Wu and Scott Rennekar

### Background

Our previous report characterized softwood thermomechanical pulp fines subjected to surface esterification (using succinic anhydride and imidazole in acetone at 40 °C for 6.25 hours) and homogenization through high-pressure micro-fluidization (referred to as SA-fines). This characterization included particle size analysis and lignin characterization. In this report, we further investigate the morphology and properties of the fines and lignin. The previous report also demonstrated that when SA-fines were cast into films via vacuum filtration through a 0.45  $\mu\text{m}$  pore-size membrane, the resulting films exhibited decent tensile strength ( $\sim 3000$  MPa compared to less than 1000 MPa for homogenized TMP fines) and modulus ( $\sim 35$  MPa compared to  $\sim 5$  MPa for homogenized TMP fines). However, the films were brittle, as indicated by a maximum strain of less than 2%. In the current study, we considered using the SA-fines as strength additives by blending them with micro/nano-fibrillated cellulose produced through mechanical refining of bleached kraft pulp (commercial product from Performance BioFilaments Inc.).

### Results

As indicated in the previous report, after esterification and homogenization, the resulting SA-fines could be fractionated (following the work by Imani et al. [1] through centrifugation at 3000g for 30 minutes) into nanoparticles (collected in the supernatant, yielding 12 wt.%) and micro-fibrillated particles at the micron scale (found in the pellet after centrifugation). We characterized the morphology of both particle types using AFM (Figure 1a) and SEM (Figures 1b–1c), respectively. The nanoparticles appeared to consist of cellulose nanofibrils and particles with a lower aspect ratio, potentially lignin nanoparticles. The larger particles collected in the centrifugation pellet displayed morphology similar to the original fines (both fibrillar and flaky shapes), though they were more fibrillated than the SEM images shown in previous reports.

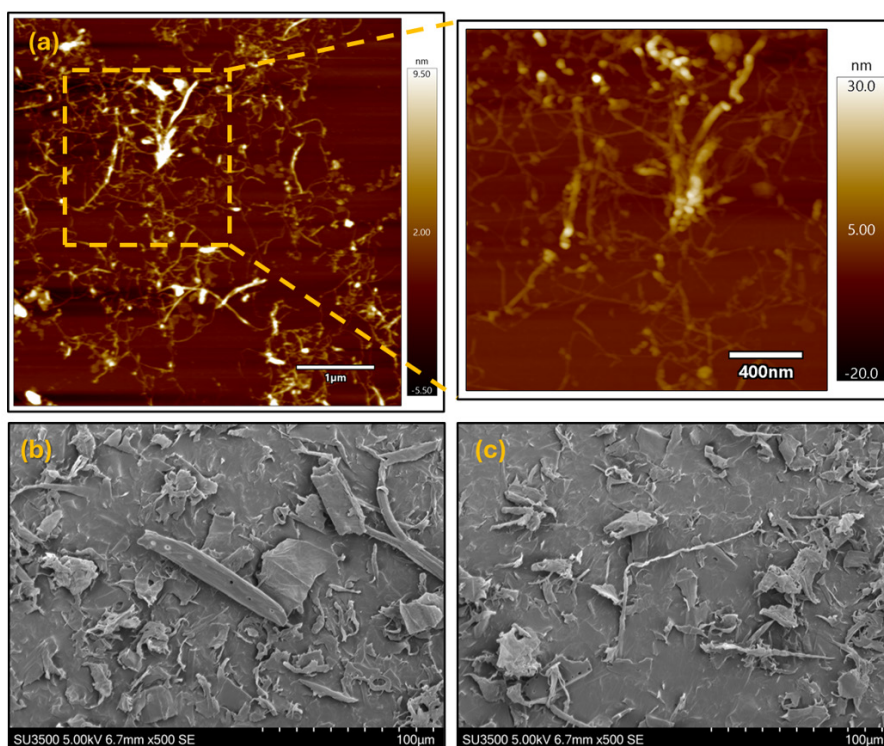


Figure 1. Morphology of nanoparticles (a) and micro-fibrillated particles (b-c) isolated from SA-fines.

The conductometric titration method was used in previous studies to assess the effect of esterification, which incorporates carboxylic acid groups (-COOH) onto the fines. In this report, we added additional measurements, including an esterification attempt without the addition of imidazole, which showed limited impact on -COOH content ( $\sim 0.15$  mmol/g). In contrast, modification with imidazole resulted in  $\sim 0.6$  mmol/g of carboxylic groups (Figure 2a). As described in the previous report, we also isolated lignin from the starting material and SA-modified fines using the MWL extraction method.

$^{31}\text{P}$  NMR analysis of MWL from SA-fines indicated a -COOH content of 1.2 mmol/g, increased from less than 0.5 mmol/g, confirming that lignin was also esterified (Figures 2b, 2e).  $^{31}\text{P}$  NMR further suggested a decrease in aliphatic -OH groups, while total phenolic -OH remained constant, indicating that

esterification occurred primarily on aliphatic -OH groups (Figures 2b, 2e). This aligns with findings in the literature showing that this regioselective esterification targets primary hydroxyl groups [2], which are located on the aliphatic side chain of lignin. The isolated lignin was then subjected to 2D HSQC NMR and GPC analyses to determine linkage types and molecular weight distribution. Results indicated that a slightly acidic environment led to lignin depolymerization, primarily through the cleavage of  $\beta$ -O-4 linkages, as evidenced by the decrease in  $\beta$ -O-4 content (Figure 2c) and reductions in both average (Figure 2d) and distribution (Figures 2f and 2g) of molecular weight in SA-MWL.

Since SA-fines did not produce flexible films on their own, they were used as strength additives by incorporating them into micro/nano-fibrillated cellulose (M/NFC) at loadings of 10, 20, 30, and 40 wt.% (Figure 3).

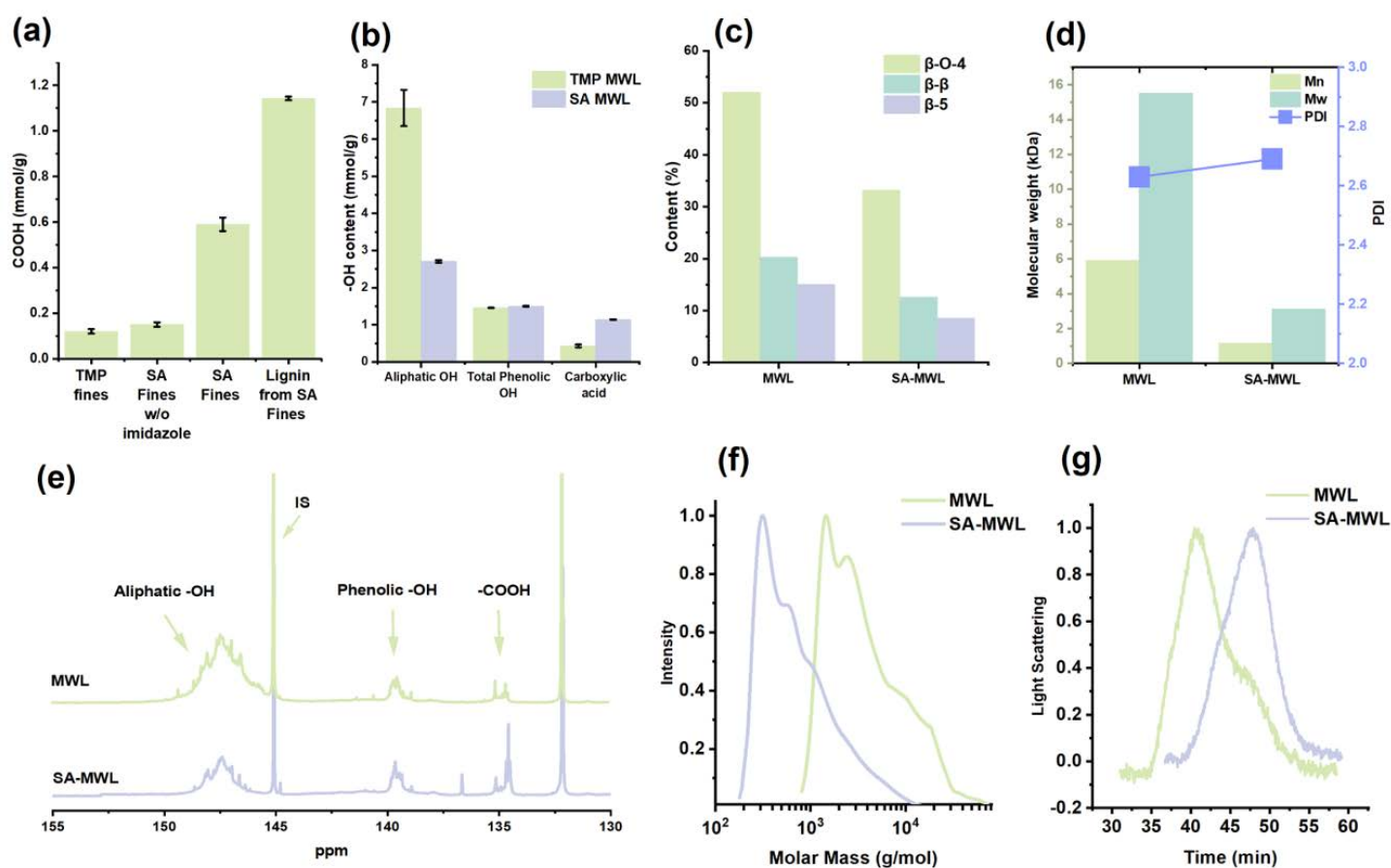


**Figure 2.** Characterization of starting and SA-fines. (a) carboxylic acid content determined by conductometric titration (fines) and  $^{31}\text{P}$  NMR (lignin) (b) hydroxyl content of lignin determined by  $^{31}\text{P}$  NMR (c) content of inherent linkages of lignin determined by 2D HSQC NMR (d) average molecular weight of lignin determined by GPC (e)  $^{31}\text{P}$  NMR spectra (f) molecular weight distribution of lignin determined by GPC (g) light-scattering spectra of lignin determined by GPC

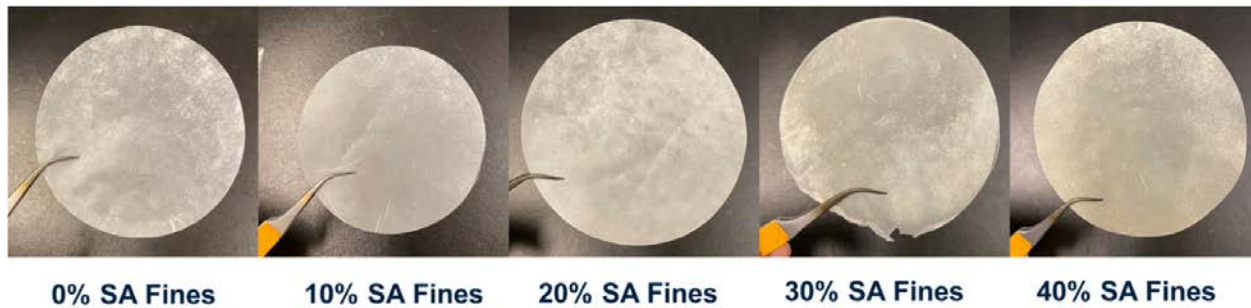


**Figure 3.** Physical Appearance of Films Derived from M/NFC with Various Levels of SA-Fines Substitution

The resulting mixtures were cast into films and subjected to tensile testing (Figure 4a-4d). The substitution of SA-fines significantly enhanced the tensile strength of M/NFC from ~35 MPa to ~60 MPa (Figure 4a). Even a 10% substitution achieved a tensile strength of 55 MPa, likely due to the improved intermolecular bonding provided by the SA-fines, which are rich in -COOH groups and capable of forming films with high tensile strength on their own. SA-fines also contributed to the stiffness of the M/NFC-derived films, though the improvement in modulus was not significant until the SA-fines loading reached 30%, increasing from ~2000 MPa to ~3500 MPa (Figure 4b). Likely due to the presence of nanofibrils (Figure 1a), the substitution of SA-fines enhanced the maximum strain of the films at 10% and 20% loadings. However, further increasing the SA-fines loading reduced this effect (Figure 4c), likely due to the insufficient presence of long fibres/fibrils in the fibre network, similar to the behaviour observed in films made solely from SA-fines.

Given the high mechanical strength, one of the potential applications of M/NFC-derived films is active packaging. The water vapour transmission rate (WVTR) and UV-blocking capability are key characteristics required for this application [3,4]. Since lignin is known to block UV light, it is anticipated that incorporating lignin-rich SA-fines into M/NFC could introduce UV-blocking functions. Thus, the transmittance of

films derived from M/NFC and SA-fines was assessed using a UV-Vis spectrometer (Figure 4e). It was apparent that the substitution of SA-fines successfully blocked UV light, with 20% substitution resulting in almost no transmittance in the 200–400 nm wavelength range. However, this also reduced the transmittance of visible light by 50%. Unlike the UV-blocking function, the M/NFC-derived film already exhibited an excellent WVTR value of 23 g/m<sup>2</sup>·h, and the substitution of SA-fines did not negatively impact this value (Figure 4f). This value is similar to that reported in a recent study on micro-fibrillated cellulose made through alkali and mechanical treatment, which demonstrated excellent capability in preserving the freshness of cherries when used as packaging material [5].

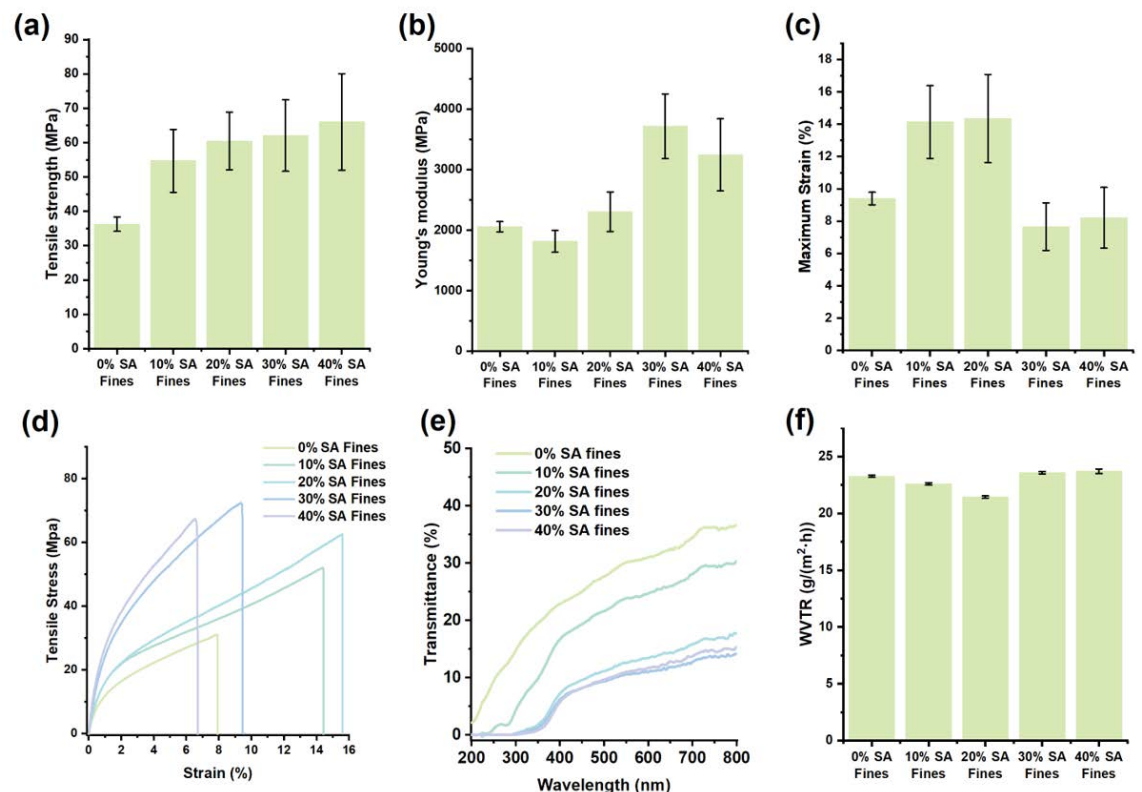


**Figure 4.** Mechanical and functional properties of M/NFC films substituted with SA-Fines (a) average value of tensile strength (b) average value of modulus (c) average value of maximum strain (d) representative stress-strain curves (e) transmittance of films from 200-800nm wavelengths (f) water vapour transmittance rate of films

In addition to films, the M/NFC used in this work is also suitable for developing other functional materials, such as aerogels. Therefore, we produced aerogels from M/NFC with various loadings of SA-fines via freeze-drying of a 1 wt.% suspension, followed by compression testing. The results indicated that the SA-fines contributed to the enhanced compressive strength of the aerogels (Figure 5), likely by increasing rigidity and improving fibre bonding.

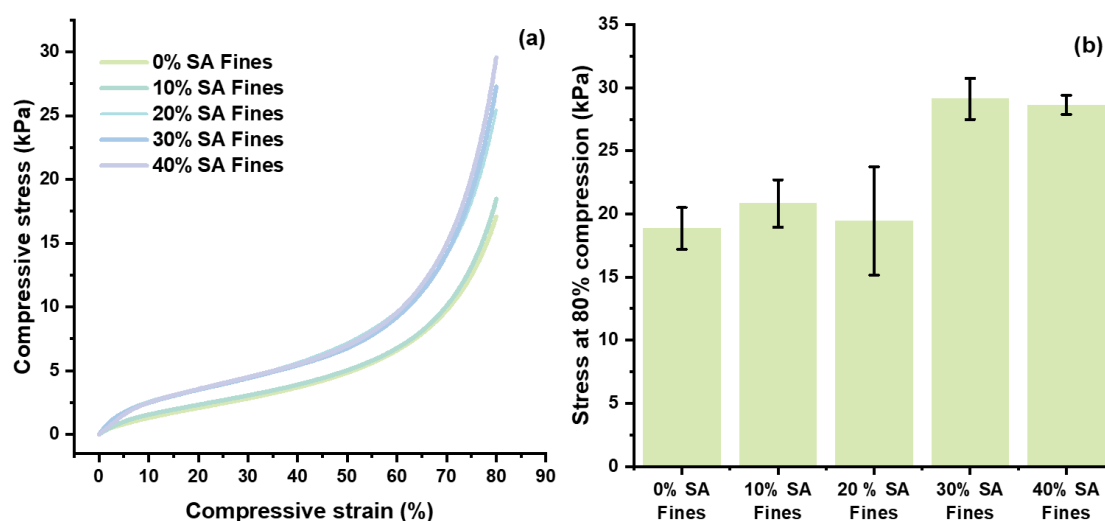


**Figure 5.** Stress-strain curves (a) and average ultimate stress at 80% compression (b) of aerogels derived from M/NFC substituted with SA-fines

## Future work

Future work will focus on further characterization of the aerogels to assess the influence of SA-fines substitution on properties such as thermal conductivity and flame retardancy. A manuscript based on the work described in the 2024 reports is currently in preparation.

## Acknowledgements

We would like to thank Kamryn Russell (undergraduate research assistant) for their valuable contributions to the experimental work of this project, Dr. Qi Hua for his assistance with lignin characterization and mechanical testing of the films, and Mr. Zhixing Huang (master's student) and Dr. Tao Zou for their help with imaging techniques.

## References

1. M. Imani, A. Ghasemian, M.R. Dehghani-Firouzabadi, E. Afra, M. Borghei, L.S. Johansson, P.A.C. Gane, O.J. Rojas, Coupling Nanofibril Lateral Size and Residual Lignin to Tailor the Properties of Lignocellulose Films, *Adv. Mater. Interfaces* 6 (2019). <https://doi.org/10.1002/admi.201900770>.
2. M. Beaumont, B.L. Tardy, G. Reyes, T. V. Koso, E. Schaubmayr, P. Jusner, A.W.T. King, R.R. Dagastine, A. Potthast, O.J. Rojas, T. Rosenau, Assembling Native Elementary Cellulose Nanofibrils via a Reversible and Regioselective Surface Functionalization, *J. Am. Chem. Soc.* 143 (2021) 17040–17046. <https://doi.org/10.1021/jacs.1c06502>.
3. Q. Hua, Z. Huang, J. Gou, H. Zhang, I. Therrien, J. Wu, Y. Liang, S. Rennecker, Harnessing the synergistic power of lignin-Ecoflex blends for enhanced performance in food packaging, *Chem. Eng. J.* 499 (2024) 156139. <https://doi.org/10.1016/j.cej.2024.156139>.
4. B. Las-Casas, V. Arantes, From production to performance: Tailoring moisture and oxygen barrier of cellulose nanomaterials for sustainable applications – A review, *Carbohydr. Polym.* 334 (2024). <https://doi.org/10.1016/j.carbpol.2024.122012>.
5. P. Zhu, A. Vo, X. Sun, Y. Zhang, M. Mandegari, S. Zargar, Q. Tu, J. Zhu, Z. Yu, H. Sun, D. Zheng, F. Jiang, Water-induced controllable deswelling strategy enabled rapid fabrication of transparent cellulose film for plastics replacement, *Chem. Eng. J.* 492 (2024) 152200. <https://doi.org/10.1016/j.cej.2024.152200>.

# PROJECT 2.2

## FROM TREES TO TREATMENT: FUNCTIONALIZING TMP EXTRACTIVES

Authors: Yimin Wang, Cameron H. M. Zheng, Laurel Schafer, Heather Trajano

### Background

Trees produce soluble molecules, or extractives, to defend against microbial or insect attacks. Project 2.2 sought to provide proof of concept for the TRL1 vision that extractives could be recovered from pulp mill process streams and transformed through hydroaminoalkylation into novel molecules for therapeutic use. Verification of this vision required identification of extractives in the pulp mill, development of a method to efficiently recover extractives from mill process streams, demonstration of hydroaminoalkylation of extractives, and evidence of therapeutic activity of aminated extractives.

First, analytical protocols were developed to determine the identity of extractives in solid process samples (e.g. pulp) and liquid process samples (e.g. whitewater). Another protocol, dependent on headspace gas chromatography-mass spectrometry (GC-MS), was developed to identify volatile compounds released from pulp or process water. Fatty acids, such as linoleic acid, and resin acids, such as abietic acid, were identified as the most abundant extractives in water samples collected throughout Meadow Lake Pulp Mill.

Hydroaminoalkylation is a reaction which adds an amine across a double bond (or olefin).<sup>1</sup> Two groups of extractives were subjected to hydroaminoalkylation during ERMP Phase 3: terpenes, found in turpentine, and linoleic acid, as a representative fatty acid. Holmen Pulp provided a sample of turpentine. Turpentine contained 57 mol%  $\alpha$ -pinene, 26 mol%  $\beta$ -pinene, and 9 mol% limonene. We demonstrated that  $\beta$ -pinene and limonene could be selectively aminated in unfractionated, or neat, turpentine. Linoleic acid contains three double bonds therefore it is a candidate for hydroaminoalkylation but its carboxylic acid group will deactivate the Schafer group tantalum-catalyst. The carboxylic acid group was removed from commercial linoleic acid by a decarbonylative dehydration reaction to produce triene, a reactive olefin with three double bonds. By applying a tantalum catalyst with a small, less sterically bulky ligand, amine groups were added to two of triene's three double bonds. The di-aminated product was accompanied by the formation of a mono-aminated product. Terpenes and linoleic acid, two types of extractives found in mechanical pulp mills, were successfully aminated.

A partnership was formed with Dr. Brent Page and Dr. Henok Sahile (UBC Pharmaceutical Sciences) to assess the therapeutic activity of aminated terpenes. MmpL3 is an essential protein for cell replication and its inhibition results in powerful antibacterial activity against *Mycobacterium tuberculosis* and *Mycobacterium abscessus*. Computer modelling, a.k.a. in silico tests, revealed that aminated  $\beta$ -pinene products had good binding affinity to protein MmpL3. Aminated  $\beta$ -pinenes are very promising for medicinal chemistry and deserve further attention.

In Summer 2024, our focus was to determine if extractives could be efficiently recovered from pulp mill streams. Extractives represent 2-5 wt% of the starting wood chips and are therefore present at low concentrations in process streams. However, Kangas and Kleen<sup>2</sup> found that fibrillar fines and flake-like fines contain a higher concentration of extractives relative to whole pulp. They also found that the surface of fibrillar fines has a high coverage of extractives suggesting that once extractives are released during pulping, they adsorb onto fines. Given these observations, we proposed that efficient extractive recovery could be achieved by the collection of fines followed by the desorption of extractives from the fines. The first objective was to establish a protocol to isolate fines from pulp mill samples to enable extractive identification and quantification. The second objective was to evaluate the impact of pH, temperature, and ionic strength on the desorption of linoleic acid from cellulose fibres.

### Materials & Methods

#### *Fines Recovery for Laboratory Analysis*

Two fines recovery protocols, illustrated in Fig. 1, were tested. Clean whitewater (CWW, provided by Meadow Lake Pulp), was added to the Britt jar with a 200-mesh screen. The Britt jar filtrate was then subjected to centrifugation or vacuum filtration in order to recover fines.

In the centrifugation method, 45 mL fines-laden Britt jar filtrate was stirred and poured into a 50 mL falcon tube, which was centrifuged at 1,000 x g force for 30 minutes. The supernatant was carefully decanted into a 50 mL falcon tube. The supernatant and fines pellet were collected for subsequent hexane extraction and GC-MS analysis (described below).

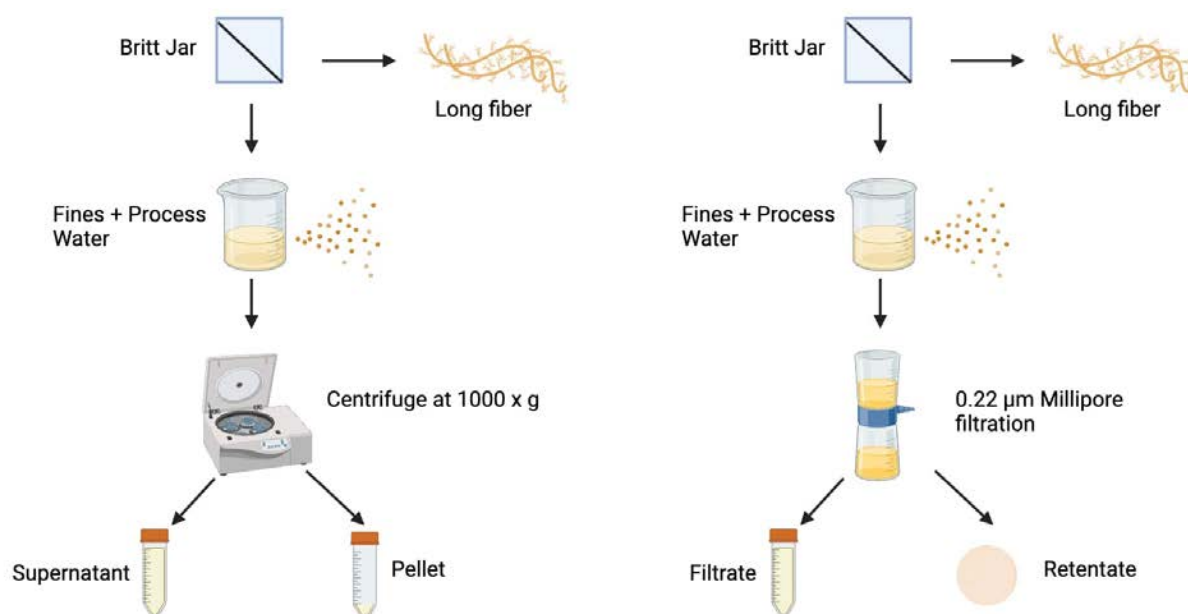


**Figure 1.** Flowchart of fines separation procedure using centrifugation (left) and Millipore vacuum filtration (right).

In the Millipore vacuum filtration method, 15 mL Britt jar filtrate was stirred and poured onto a 0.22 µm Millipore filter paper and vacuum was applied. Fines sized 0.22 µm to 76 µm (the mesh size of Britt Jar) were retained on the filter paper. This procedure was repeated a total of three times in order to collect sufficient Millipore filtrate and fines retentate for hexane extraction and GC-MS analysis (described below).

#### *Desorption of linoleic acid from cellulose filter paper*

Due to time constraints and challenges in quantifying extractive concentration in mill samples, it was decided that extractive recovery from fibres should be studied using a model system: purified linoleic acid adsorbed on Whatman filter paper. To adsorb linoleic acid onto Whatman 1 cellulose filter paper (CAS # 1001-150), 3 µL linoleic acid was streaked onto one-eighth of a 150 mm diameter filter paper using a P10 pipette tip and incubated overnight at 4 °C. The linoleic acid-filter paper was then incubated in 40 mL distilled water in a 50 mL falcon tube for 40 minutes. Three experimental campaigns were conducted to test the effect of pH, temperature, and ionic strength. Temperature was kept at 40°C when pH was varied to pH 4, 7, and 10. pH was kept at 7 when temperature was varied to 25 °C, 40 °C and 55 °C.

Finally, at pH 7 and 40 °C, ionic strength was varied by adding 1M NaCl and 1M CaCl<sub>2</sub>. After incubation, the filter paper was carefully transferred to a new 50 mL falcon tube for extraction with hexanes and GC-MS (described below). The filter paper was subjected to hexane extraction as it was simpler than liquid-liquid extraction of desorption water with hexanes.

#### *Hexanes Extraction and GC-MS Analysis*

Liquid samples (e.g. centrifuge supernatant, Millipore filtrate) were subjected to liquid-liquid extraction with 40 mL of hexanes at 25 °C. Solid samples (e.g. fines pellet, fines retentate, cellulose filter paper) were extracted with 40 mL hexanes at 25 °C. After extraction, the hexane fraction was collected and mixed with MgSO<sub>4</sub> to remove all residual water. The hexanes extracts were dried in a rotary evaporator, subjected to trimethylsilyl (TMS) derivatization to enhance compound volatility, and analyzed by gas chromatography-mass spectrometry with an HP-5 ms (30 m×0.25 mm×0.25 µm) column in UBC's Core Analytical Facility. Hexadecane was used as an internal standard for GC-MS. Each chromatogram peak represents a unique molecule and the larger the peak, the greater the molecule's concentration in the sample.

## Results

### Fines Recovery for Laboratory Analysis

Chromatograms of hexane extracts of CWW supernatant, pellet, Millipore filtrate, and Millipore retentate are presented in Figure 2. The area of each extractive peak was normalized to the total chromatogram peak area; only species with a relative area greater than 1% were searched in the NIST library and reported in Table 1. The two most abundant extractives in each fraction are italicized. When centrifugation is employed, the CWW fines (pellet, panel a) contain fewer extractives at a lower concentration than the process water (supernatant, panel c). All extractives identified in the pellet were also present in the supernatant; we suspect that this was due to the residual liquid retained by the pellet.

By contrast, when Millipore vacuum filtration was employed, the fines fraction (panel b) contained a greater number of extractives at higher concentrations than the process water (panel d). The process water filtrate contained abietic acid and isopimaric acid, which were also found in the fines retentate along with several other acids. The differences between extractives distribution after centrifugation and filtration require examination in future studies. However, Millipore vacuum filtration was the preferred method as it resulted in less water remaining with the retentate, better retention of fines, and greater certainty of fines size. Pouring out supernatant after centrifugation easily disturbed fibrillar fines and complete separation between the process water and fines pellet could not be achieved due to unavoidable residual liquid in the pellet.

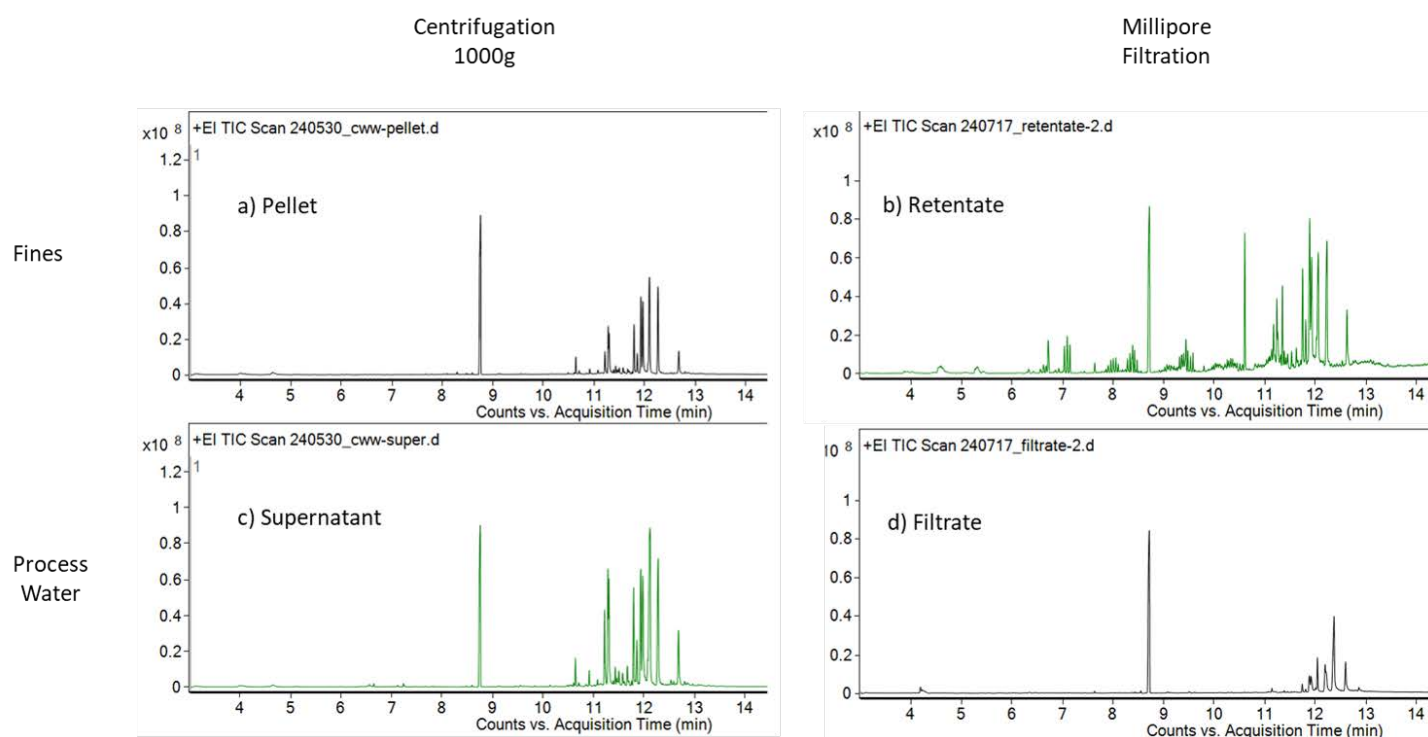


**Figure 2.** GC-MS chromatograms of hexanes extracts of Meadow Lake Pulp Mill clear whitewater (CWW). Centrifugation was used to separate fines as a pellet (panel a) from aqueous supernatant (panel c). Millipore filtration was used to separate fines as retentate (panel b) from aqueous filtrate (panel d). Hexadecane, the internal standard, appears at a retention time of 8.7 minutes.

**Table 1.** Extractives identified in CWW from Meadow Lake Pulp. CWW was fractionated into fines and process water by centrifugation or by Millipore vacuum filtration. Extractives in red italics were the two most concentrated species.

Centrifugation 1000g		Millipore Vacuum Filtration	
Fines Pellet	Process Water Supernatant	Fines Retentate	Process Water Filtrate
<i>Abietic acid</i>	Abietic acid	<i>Abietic acid</i>	<i>Abietic acid</i>
<i>Dehydroabietic acid</i>	<i>Dehydroabietic acid</i>	Dehydroabietic acid	
Isopimaric acid	Isopimaric acid	<i>Isopimaric acid</i>	<i>Isopimaric acid</i>
Pimaric acid	<i>Pimaric acid</i>	Pimaric acid	
Oleic acid	Oleic acid	Oleic acid	
Linoleic acid	Linoleic acid	Linoleic acid	
	Oxodehydroabietic acid		

### *Desorption of linoleic acid from cellulose filter paper*

pH, temperature, and ionic strength were varied in order to identify conditions which promoted linoleic acid desorption from cellulose filter paper. As it was the post-desorption filter paper that was subjected to hexanes extraction, a smaller linoleic acid peak indicates greater desorption of linoleic acid from cellulose.

The effect of pH was tested (Figure 3a/b/c). Desorption at 40 oC and pH 4 produced the smallest linoleic acid peak indicating the least amount of linoleic acid remaining on the cellulose. Desorption at pH 7 produced the largest peak. These results contradict previous tests, performed at 80 oC, where pH 7 was more effective in extracting linoleic acid than pH 4 (Steering Committee Meeting, June 2022). The large temperature difference

could play a role in this discrepancy. Further testing is required to verify these observations.

The greatest desorption was observed at 25 °C, the extent of desorption decreased as temperature increased (Figure 3d/e/f). It was expected that increasing temperature would increase the rate of mass transfer due to increased diffusion. Amanpour et al.<sup>3</sup> observed oxidation of linoleic acid into volatile compounds at 60 °C but our previous work to remove linoleic acid from whole pulp was conducted at 80 °C. Further investigation of the temperature dependence of linoleic desorption and oxidation is required.

Lastly, the effect of ionic strength was tested by adding 1M NaCl or 1M CaCl<sub>2</sub> (Figure 3g/h/i) to distilled water. The addition of salt increased desorption of linoleic acid relative to distilled water.

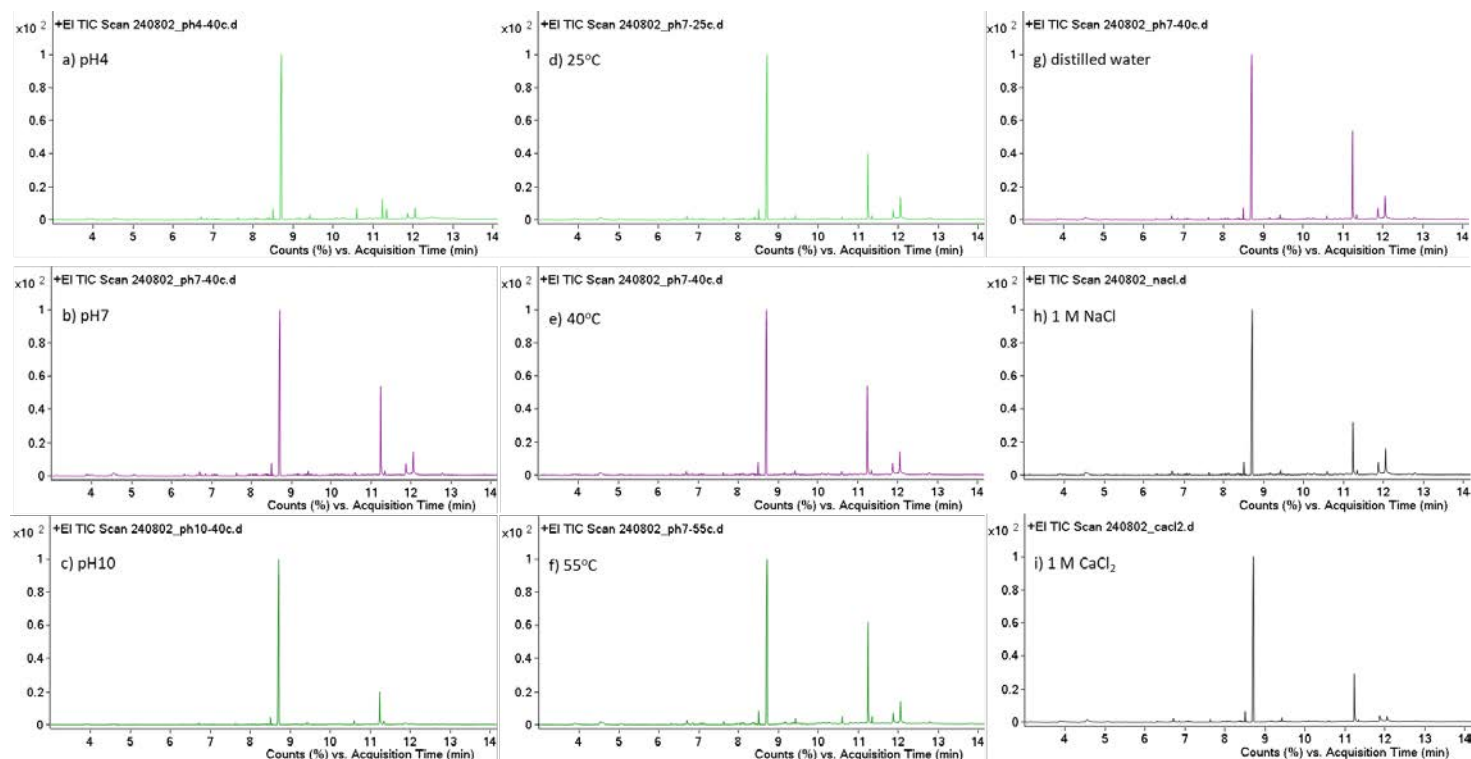


**Figure 3.** GC-MS chromatogram of hexanes extraction of linoleic acid on Whatman 1 filter paper after water desorption for 40 minutes. Effect of pH at 40oC was tested at pH4 (panel a), pH7 (panel b), and pH10 (panel c). Effect of temperature at pH7 was tested at 25 oC (panel d), 40 oC (panel e), and 55 oC (panel f). Effect of ionic strength at 40oC and pH 7 was tested with distilled water (panel g), 1M NaCl (panel h), and 1M CaCl<sub>2</sub> (panel i). Hexadecane, the internal standard, appears at a retention time of 8.7 minutes. Linoleic acid appears at a retention time of 11.23 min.

# PROJECT 2.2

## Conclusions & Future Work

A laboratory protocol to separate fines from mill samples by Millipore filtration was achieved. Clear whitewater fines contained a greater number of extractives at higher concentration than the water which supports the vision of collecting fines as the first step of extractives recovery in mechanical pulp mills. Modification of pH, temperature, and ionic strength affected the degree of desorption of linoleic acid from cellulose fibres. Desorption of linoleic acid from cellulose was most effective at acidic pH, low temperature, or high ionic strength.

ERMP 3 began with a TRL1 vision to transform extractives, recovered from mechanical pulp fines, into novel therapeutic molecules. This vision has been advanced to TRL2. Analytical protocols were established and used to identify extractives and their volatile derivatives in-process samples. A laboratory protocol to separate fines from mill samples was achieved and

used to identify a high concentration of extractives in the fines. Extractives can be desorbed from cellulose fibres by adjusting suspension conditions. Commercial linoleic acid and neat turpentine were aminated using tantalum catalysts. In silico tests verified that aminated  $\beta$ -pinene products are promising starting points for medicinal chemistry. These encouraging results all point to the need for further work to advance the vision of producing novel, high-value chemicals from extractives in mechanical pulp mills. The experiences gained during this project have created a strong foundation for launching future efforts.

## Acknowledgements

We thank Dr. Harley Gordon and Dr. Eerik Piirtola of the Analytical Core Facility in the UBC Faculty of Land and Food Systems for sharing their expertise on GC-MS.

## References

1. Edwards, P. M.; Schafer, L. L. *Chem. Commun.* 2018, 54, 12543–12560.
2. Kangas, H.; Kleen, M. *Nordic Pulp & Paper Research Journal*, 2004, 19(2), 191-199.
3. Amanpour, A.; Kelebek, H.; Kesen, S.; Selli, S. *J Am oil Chem Soc*, 2016, 12 (2016): 1595-1603.

# PROJECT 2.3

## PRODUCTION, CHARACTERIZATION, AND APPLICATIONS OF MFC DERIVED FROM MECHANICAL PULP FINES

Authors: Mariana Frias de Albuquerque, James Olson, Boris Stoeber, Heather Trajano

### Background

This project aims to reduce the energy required to produce microfibrillated lignocellulose (MFLC) from mechanical pulp fines for various paper applications by incorporating enzymatic hydrolysis before refining. In earlier phases, we explored the production of MFLC using short fibres derived from softwood bleached chemi-thermomechanical pulp (BCTMP). The pulp was fractionated through a 0.8 mm hole screen and refined at the UBC Pulp and Paper Centre pilot plant. These refined short fibres were blended with long fibres to form paper handsheets, demonstrating that the short fibres improved tensile strength while the long fibres enhanced bulk (Seifert et al. 2023). We also correlated specific refining energy with the rheological properties of fibre suspensions, observing how refining influenced the elasticity of short fibres. Subsequently, the enzymatic hydrolysis of short BCTMP fibres was examined under different pH and temperature conditions to assess their impact on fibre morphology and inter-fibre interactions after PFI-refining. Higher incubation temperatures softened fibre structures, facilitating fibrillation, while alkaline pH conditions enhanced surface charge modifications, enabling enzymes to act more effectively on the microfibrillar structure (Frias et al. 2024). Further work evaluated the interaction between hydrolysis duration and enzyme dosage, identifying a balance between enzyme load and process time for achieving specific fibrillation and fibre length targets.

Our last report discussed the enzymatic treatment of non-fractionated BCTMP fibres to broaden the scope of fibre lengths undergoing hydrolysis. Whole pulp was incubated with endoglucanase at pH 5 and 60 °C for 2 hours, followed by refining using a PFI mill (0 to 5,000 revolutions). Hydrolysis effects were limited, primarily due to low cellulose accessibility, with no significant reduction in average fibre length. However, treated fibres exhibited a higher kink index than untreated fibres across all refining levels, suggesting enzymatic cleavage of bonds along the fibres without promoting excessive cutting during refining. Enzymatic hydrolysis and refining reduced CSF values due to increased fines fraction generation (Frias et al. 2024).

Since our last committee meeting, we have worked on scaling up the enzymatic hydrolysis process from laboratory to pilot plant scale. Modifications to the hydrolysis protocol were implemented to accommodate larger volumes of pulp, and refining post-hydrolysis was compared between the PFI mill and low-consistency refining. These comparative results, along with observations on scaling, are further detailed in this report.

### Results

For the last few months, we have advanced the scale-up of enzymatic hydrolysis of BCTMP with endoglucanase as a pretreatment step preceding refining. A challenge identified during this process was the requirement for large volumes of buffer solutions to achieve a target incubation pH. In an industrial pulp mill context, adding such volumes would significantly increase operational costs and potentially introduce complications in downstream processes, including water purification and waste management. We first evaluated the feasibility of performing enzymatic hydrolysis in reverse-osmosis (RO) water without pH adjustment at the laboratory scale to address this issue. We then transitioned the process to the pilot plant scale. The results and implications of these experiments at both scales are presented in the following sections.

#### *PFI refining of hydrolyzed BCTMP fibres*

30 oven-dried grams (ODg) of BCTMP were incubated with 0 wt.% and 0.1 wt.% endoglucanase (EN) at 60°C in RO water, with the suspension maintaining an overall pH of 8.9 for 2 hours. After hydrolysis was stopped, the fibres were washed with 1 L of RO water. Subsequently, 24 OD grams of the pulp were refined using a PFI mill, with samples collected at 0, 1,000, 5,000, and 10,000 revolutions. The fibres were then characterized using a Fiber Quality Analyzer (FQA) to assess fibre morphology, and the fines content, defined as particles smaller than 75 µm, was determined using a dynamic drainage jar (DDJ). Fig. 1 presents the FQA measurements of fibre morphology, including length-weighted fibre length and fines content, alongside the fines content determined using the DDJ.

## PROJECT 2.3

The low intensity of the PFI mill (Kerekes 2005) resulted in minimal fibre length reduction for samples incubated without enzymes, with only a 6% decrease in length observed after 10,000 revolutions compared to unrefined, unhydrolyzed pulp (Fig.1-a). In contrast, fibres incubated with 0.1 wt.% EN exhibited a progressive reduction in length with increasing refining intensity, resulting in a 15% reduction after 10,000 revolutions. This indicates that enzymatic hydrolysis promoted fibre cleavage, facilitating the refining action. Analysis of fibre length distributions from the FQA revealed mass transfer: the fraction of longer fibres (1.0–5.0 mm) decreased with refining, while shorter fibres (0.2–1.0 mm) became more predominant, further supporting the impact of EN on fibre structure.

The FQA defines fines as particles smaller than 0.2 mm but larger than 70  $\mu\text{m}$ , while the DDJ captures particles smaller than 75  $\mu\text{m}$ , corresponding to those that pass through a 200-mesh screen. These measurements can be complementary, offering a more comprehensive understanding of fines generation.

For unhydrolyzed fibres, refining does not significantly increase “FQA fines” (Fig. 1-b), reflecting the limited reduction in fibre length. However, “DDJ fines” content increases steadily with refining up to 5,000 revolutions, suggesting the release of surface material such as fibrils and particulate fines (Fig. 1-c). Beyond 5,000 revolutions, a 20% decrease in DDJ fines is observed. This reduction could be attributed to fines agglomeration, making them too large to pass through the mesh, or to the entrapment of fines on fibres due to external fibrillation (Gharekhani et al. 2015).

Hydrolyzed fibres generated more FQA fines compared to unhydrolyzed fibres. Between 0 and 1,000 revolutions, there is a slight reduction in FQA fines and an increase in DDJ fines. This trend may result from the enzymatic unravelling of the fines structure, as highlighted in our last newsletter, which allows fibrils to pass through a 200-mesh screen without being detected by the FQA. Beyond this initial stage, FQA fines increase, primarily due to the cutting of fibres during refining. In contrast, DDJ fines remain relatively consistent between 1,000 and 10,000 revolutions, suggesting that fines generation stabilizes or that further refining does not significantly impact DDJ fines. Compared to results from our last study (Frias et al. 2024), incubating BCTMP with EN in RO water without pH adjustment resulted in a more pronounced reduction in fibre length than at pH 5. However, incubation at pH 5 generated more DDJ fines with refining, significantly influencing drainage properties.

Given the demonstrated enzymatic activity and fibre morphology change without pH modifications, the process was subsequently scaled up to pilot plant trials, as detailed in the following section.

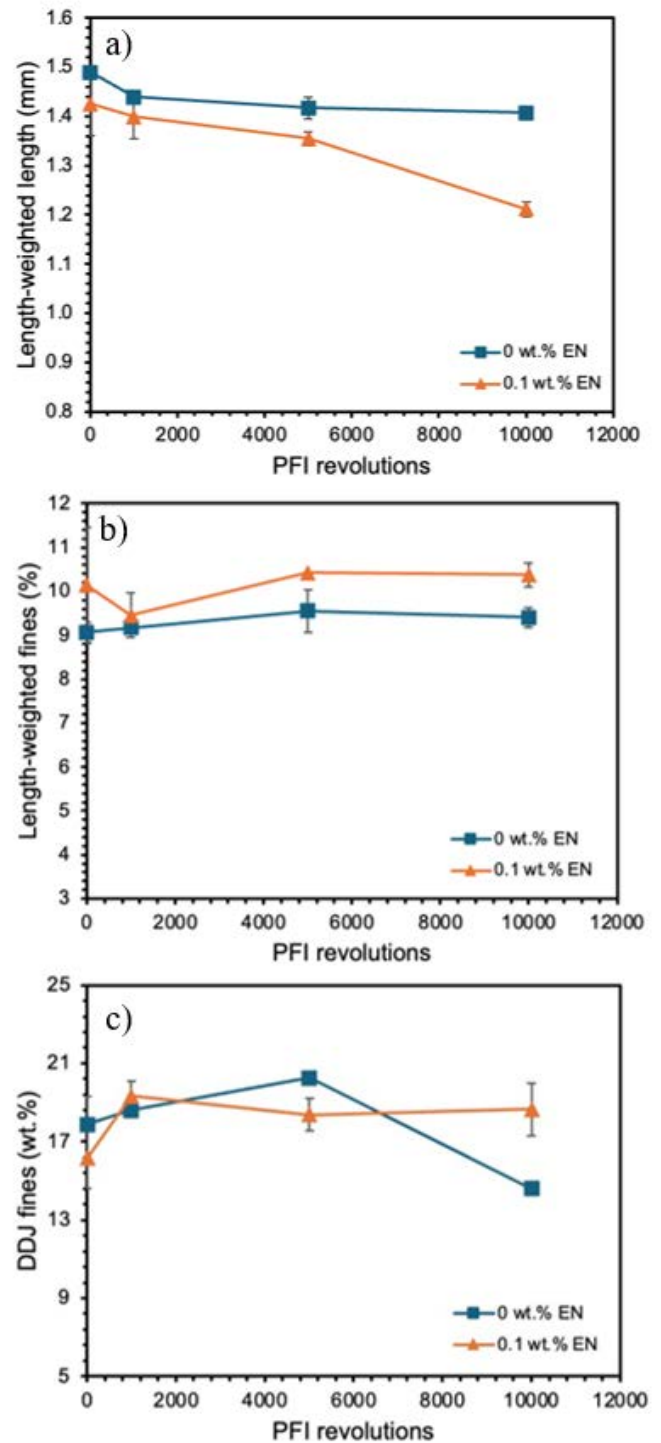


**Figure 1.** Length-weighted length (a), fines content (b), and Dynamic Drainage Jar fines content (c) of PFI-refined BCTMP fibres incubated with 0 wt.% and 0.1 wt.% endoglucanase (EN).

## LC refining of hydrolyzed BCTMP fibres

7.7 OD kilograms of BCTMP were incubated with 0 wt.% and 0.1 wt.% EN at 60 °C for 2 hours at a consistency of 3.5%, with the suspension pH maintained at 8.9. The incubation was conducted in the repulper tank of the pilot plant facility at the UBC Pulp and Paper Centre, where continuous mixing was applied to enhance enzyme diffusion. Temperature was regulated using three submersible heaters. The hydrolysis reaction was stopped by adding a chlorine solution at a concentration of 10 ppm, based on the OD weight of the pulp. The treated fibres were subjected to LC refining using an AIKAWA single-disk 14" refiner. Samples were collected at approximately 0, 120, 200, 260, and 330 kWh/ton energy levels. Fibre morphology was characterized using an FQA, and the fibres were observed under an optical microscope (Nikon Optiphot) to visualize fibrillation and evaluate the effects of enzymatic hydrolysis on refining performance. Handsheets were prepared at each refining stage, and their mechanical properties were tested. Fig. 2 presents the FQA characterization of length-weighted length and fines content for LC-refined BCTMP fibres, both with and without enzymatic hydrolysis pre-treatment.

Unhydrolyzed fibres exhibited progressive fibre cutting with increased refining energy, a typical characteristic of LC refining (Fig. 2-a). In contrast, fibre shortening in hydrolyzed fibres was more pronounced due to the enzymatic modification of their structure. EN weakens the fibre structure by randomly cleaving internal bonds in cellulose molecules. This fibre cutting is reflected in the increased generation of fines (Fig. 2-b) for hydrolyzed fibres. In contrast, unhydrolyzed BCTMP exhibited an energy threshold beyond which fines generation remained limited, possibly due to increased external fibrillation still attached to the fibres. Optical images (Fig. 3) reveal increased external fibrillation in unrefined, hydrolyzed fibres. At 334 kWh/ton, fibres treated with EN appear shorter than unhydrolyzed fibres, with a higher presence of fibrillar fines and fibre fragments.

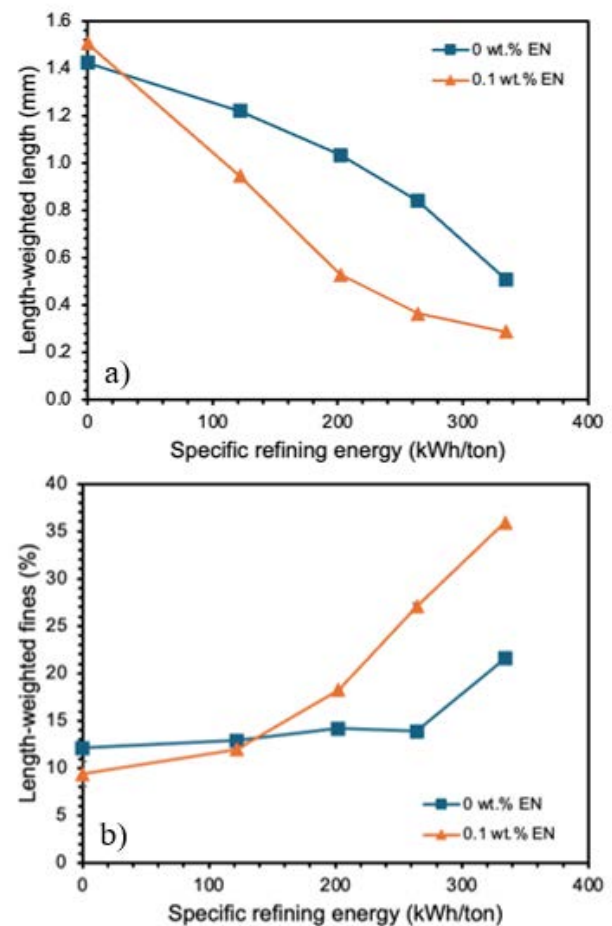
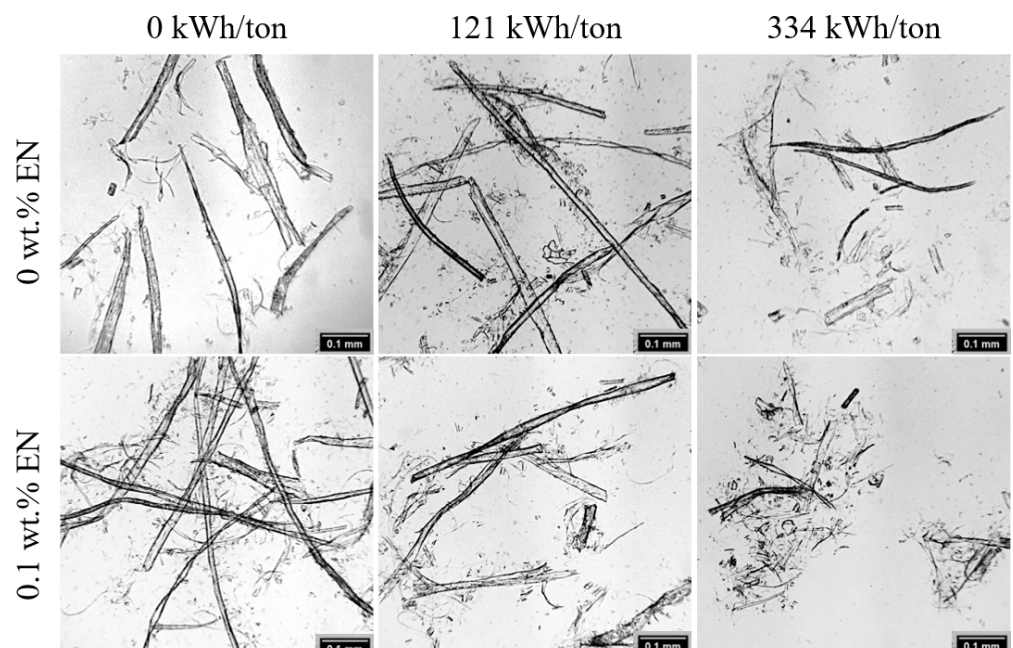


**Figure 2.** Length-weighted length (a) and fines content (b) of LC-refined BCTMP fibres incubated with 0 wt.% and 0.1 wt.% endoglucanase (EN).

**Figure 3.** Optical microscopy images of BCTMP fibres incubated with 0 wt.% and 0.1 wt.% endoglucanase (EN), LC-refined at 0 kWh/ton, 121 kWh/ton, and 334 kWh/ton.



## PROJECT 2.3

Finally, Fig. 4 illustrates the progression of handsheet properties with specific refining energy for unhydrolyzed and hydrolyzed fibres. Consistent with fibre shortening, bulk and tear index decrease with increasing refining energy (Fig. 4-a, c) – more prominently for fibres pre-treated with EN. The reduction in tear index for hydrolyzed fibres is attributed to their shorter length, as tear resistance heavily depends on fibre length (Page and Macleod 1992). While refining generates fines that enhance sheet density and bonding, these fines contribute minimally to tear strength. Fig. 4-b demonstrates that handsheet tensile strength increases similarly for both hydrolyzed and unhydrolyzed fibres up to 220 kWh/ton. However, at 334 kWh/ton, handsheets made from EN-treated fibres exhibit a 10% higher tensile index than those from unhydrolyzed fibres.

The intensified effect of enzymatic hydrolysis under LC refining is evident in Fig. 4-d, where elasticity modulus increases more rapidly for hydrolyzed fibres up to 220 kWh/ton but decreases at 334 kWh/ton. This trend suggests a nuanced interplay between fibre flexibility and strength. Enzymatic hydrolysis likely weakens the inherent strength of individual fibres, enabling easier deformation and enhancing elasticity. However, this weakening

may constrain further tensile strength gains, resulting in a relative shift favouring elasticity over strength as refining progresses. EN promotes an enhanced elasticity that may stem from increased fines generation, improved fibre reactivity, and greater accessibility of cellulose. Previous studies have highlighted that endoglucanases can reduce the molecular weight and viscosity of pulp and increase micropore volume when combined with refining (Rahikainen et al. 2019). These effects could enhance the flexibility and bonding potential of fibres, contributing to the observed increase in elasticity. Although those studies primarily focused on kraft pulp, which presents fewer inhibitors to EN activity than mechanical pulp, the findings provide valuable insights. The enzymatic hydrolysis effect observed in this study could extend to regions where EN has successfully bound to mechanical pulp fibres, modifying their structure and increasing the elasticity of formed handsheets. Incorporating enzymatic hydrolysis before LC refining offers opportunities for tailoring paper properties, as hydrolyzed fibres exhibit distinct responses to refining. Additionally, this approach can reduce the energy required for fibre shortening and the generation of fibrillar fines, aligning with process efficiency goals.

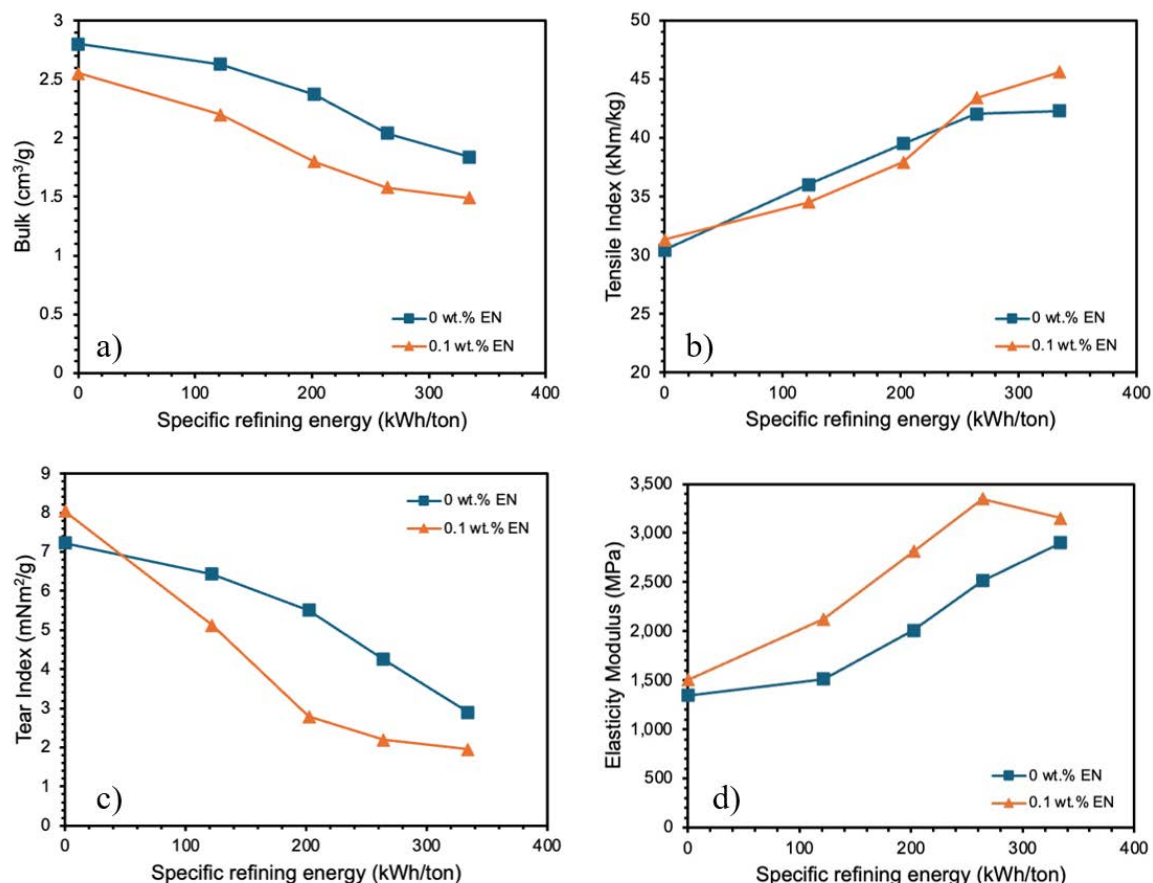


**Figure 4.** Bulk (a), tensile index (b), tear index (c), and elasticity modulus (d) of handsheets prepared from LC-refined BCTMP fibres, previously incubated with 0 wt.% and 0.1 wt.% endoglucanase (EN). 27

## Future work

In the following steps, we will analyze the handsheet properties of hydrolyzed BCTMP samples refined using the PFI mill, as detailed in the previous section. By comparing the effects of PFI and LC refining on fibres post-hydrolysis, we aim to elucidate the mechanisms by which endoglucanase alters the structure of BCTMP fibres. Additionally, we will extend this comparison to aspen BCTMP, in contrast to the softwood blend (spruce, fir, and pine) analyzed in this newsletter. Laboratory and pilot plant trials for aspen BCTMP have already been completed. Finally, Mariana will finalize her PhD thesis, consolidating the findings shared with the ERMP Phase 3 cohort throughout this project.

## References

1. Frias, M., Reynoso, S. Rambhia, S., Noki, G., Olson, J., Stoeber, B., Trajano, H. L. "Effect of Incubation Conditions of Cellulase Hydrolysis on Mechanical Pulp Fibre Morphology." (2024) *Carbohydrate Polymers* 344:122529. doi: 10.1016/j.carbpol.2024.122529.
2. Frias, M. Trajano, H. L., Stoeber, B., Olson, J., "Effect of Enzymatic Hydrolysis on the Refining of Mechanical Pulp Fibres." in IMPC 2024; Sundsvall, Sweden
3. Gharekhani, S., Sadeghinezhad, E., Kazi, S., Yarmand, H., Badarudin, A., Safaei, M. R. Zubir. N. "Basic Effects of Pulp Refining on Fiber Properties—A Review." (2015). *Carbohydrate Polymers* 115:785–803.
4. Kerekes, R. J. (2005). "Characterizing Refining Action in PFI Mills." *Tappi Journal* 4(3):9–14.
5. Page, D., and J. M. Macleod. (1992). "Fiber Strength and Its Impact on Tear Strength." *Tappi Journal*.
6. Rahikainen, J., Ceccherini, S., Molinier, M., Holopainen-Mantila, U., Reza, M., Väisänen, S., Puranen, T., Kruus, K., Vuorinen, T., Maloney, T. Suurnäkki, A., Grönqvist, S. "Effect of Cellulase Family and Structure on Modification of Wood Fibres at High Consistency." (2019) *Cellulose* 26(8):5085–5103.
7. Seifert, R., Gharekhani, S., Vargas Figueroa, D., Mercur, J., & Olson, J. "Engineering the paper production by combined fibre fractionation and reinforcement with microfibrillated cellulose" (2023). *Cellulose*, 30(5), 3201–3217.

# PROJECT 2.3B

## INCORPORATING MICRO-FIBRILLATED LIGNOCELLULOSE FOR HIGH STRENGTH AND HIGH BULK PAPER

Authors: Fariba Yeganeh, Michael A. Bilek, James Olson.

### Background

Thermo-mechanical pulp (TMP), made by refining wood chips with steam, is vital in paper manufacturing for newsprint, printing paper, and packaging. It accounts for 20-25% of global production and is prized for its high yields of 90-98% (Areej et al. 2023). Low consistency (LC) pulp develops mechanical pulp fibre properties for papermaking through facilitating water absorption, inducing fibrillation for increased surface area, and promoting cell wall delamination for fibre flexibility, and results in denser and stronger paper sheets (Bajpai 2018). TMP products are known for their high bulk, low cost, and stiffness due to retained lignin (Bajpai et al. 2018). However, mechanical pulp papers often lack strength, at a given porosity and bulk, due to lignin interfering with fiber bonding and fiber shortening during refining (Fernandez et al. 2018). Various refining and fibre fractionation systems have been explored to expand the properties of mechanical pulps (Lemrini et al. 2015; Miller et al. 2017; Rubiano Berna et al. 2019). Studies showed that reinforcement agents like fines and micro/nano-fibrillated cellulose are promising for enhancing paper strength, especially, micro-fibrillated lignocellulose (MFLC) that is comprised of lignocellulosic fibrils from mechanical pulps. (Bharimalla et al. 2017; Jahangir and Olson 2020; Kargupta et al. 2021; Khan et al. 2014; Shafiei-Sabet et al. 2016).

This study aimed to utilize LC refining to produce MFLC and create high-bulk composite sheets. We tested the reinforcement potential of MFLC by blending it with BCTMP-SPF whole fibres and long fibre fractions at different ratios. Our goal was to develop high-bulk sheets with improved properties for packaging applications while ensuring a cost-effective and sustainable approach with minimal energy use during the refining process.

### Summary of Work Done

#### *LC Refining Trials*

Two LC refining trials were conducted using an Aikawa-14" single disc refiner: one for producing LC-refined sheets with BCTMP-SPF and another for MFLC with BCTMP-aspen. Refining was done in a continuous recirculating loop with a flow rate of

250 L/min and a rotational speed of 1200 rpm. The objective was to achieve high specific refining energy (SRE), with BCTMP-aspen refined to ~1600 kWh/t and BCTMP-SPF to 545 kWh/t. Six samples were collected during the BCTMP-SPF trial at different SREs with about 100 kWh/t intervals.

#### *Composites Handsheets Preparation*

Two types of composite handsheets with a targeted grammage of 60 g/m<sup>2</sup> were made by TAPPI T 205 standard (Tappi 2002) by blending 0- 20% MFLC with SPF fibres: one with whole fibres and one with long To achieve long fibres, SPF fibres were fractionated using a Bauer-McNett classifier. Handsheets were made using a mechanical sheet maker with a recirculation loop to retain MFLC. The sheets were air-dried in a controlled temperature and humidity room at 25 ± 2 °C and 50 ± 3% humidity for 24 hr prior to testing (TAPPI 2013). All sheets were characterized for bulk, tensile strength and tear strength.

### Results

Increasing SRE improved the tensile index and tensile energy absorption (TEA). The highest values were achieved with the LC-refined pulp at 545 kWh/t. Increasing SRE develops the tensile index and TEA by beating fibres and breaking down fibres in fines (Seifert et al. 2023). Although highly LC-refined pulp led to higher tensile strength, it resulted in low bulk and also excessive energy was consumed during re-pulping.

Incorporating MFLC into both whole pulp and long fibres improved tensile strength. Long fibres that mainly contribute to bulk development, led to high bulk composite sheets while the composites produced from whole pulp and MFLC displayed higher tensile index and TEA. This can be attributed to the influence of fines on the tensile index, alongside the enhanced fibre-fibre binding by MFLC (Brodin and Eriksen 2015). In the composites formed of whole pulp and MFLC, the preservation of fines, along with the reinforcement of the fibre network by MFLC, enables the fibres to withstand higher stress levels, resulting in an increased tensile index and TEA.

## PROJECT 2.3B

Results also showed that the tear index decreased as SRE increased due to the occurrence of fibre shortening (Luukkonen et al. 2010; Elahimehr et al. 2015). Adding MFLC to long fibres significantly increased tear strength, while MFLC addition to the whole pulp, did not notably reinforce the tear strength of the resulting composites. This indicates the preservation of fibre length alongside the addition of MFLC-enhanced inter-fibre bonding, increasing the tear strength. The composites made from whole pulp and MFLC contained short fibres and fines, and they likely reached maximum tear resistance, and the additional MFLC did not contribute to further improvement. However, composites produced from whole pulp and MFLC showed a higher tear index than those made from long fibres and MFLC, indicating the positive impact of bond strength and fibre network on tear index in addition to fibre length. In the comparison between the composite sheets and the LC-refined sheets at an equivalent SRE, composite sheets showed a higher tear index and bulk. The addition of MFLC contributed to enhanced tear strength without significantly reducing bulk. These findings underscored that MFLC addition not only improves the tear strength of the composites but also could help reduce the energy required to produce high-strength sheets.

### *Extended Methodology: Increased MFLC Content*

Previous results demonstrated that MFLC addition positively affects the properties of composite sheets, we now aimed to increase the MFLC content up to 70%. An additional set of experiments was conducted to investigate the impact of higher MFLC percentages on composite sheet properties.

### *Extended Results: Tensile Index and Tear Index*

Results showed adding MFLC to SPF-whole pulp and SPF-long fibres increased tensile strength TEA while reducing bulk. This improvement is not due to increased fibre flexibility, but rather to enhanced fibre-fibre bonding and the bridging of fibrils across fibres by the MFLC (Brodin and Eriksen, 2015). When the MFLC percentage increased from 30% -70% it formed a microfibril network that could provide additional strength and enhance tensile properties. This could increase the sheets' ability to withstand higher stress levels by distributing the load across more fibres and bonds. When the MFLC content increased to 70%, the tensile strength of whole pulp and long fibre composites became similar, indicating that at high MFLC concentrations, the tensile strength is primarily governed by the MFLC network, as shown in Figure. 1. When comparing composite sheets to LC- refined sheets, MFLC added to SPF- long fibres and SPF- whole pulp

increased tensile strength, but the enhancement was similar to that achieved by LC- refining of SPF whole pulp.

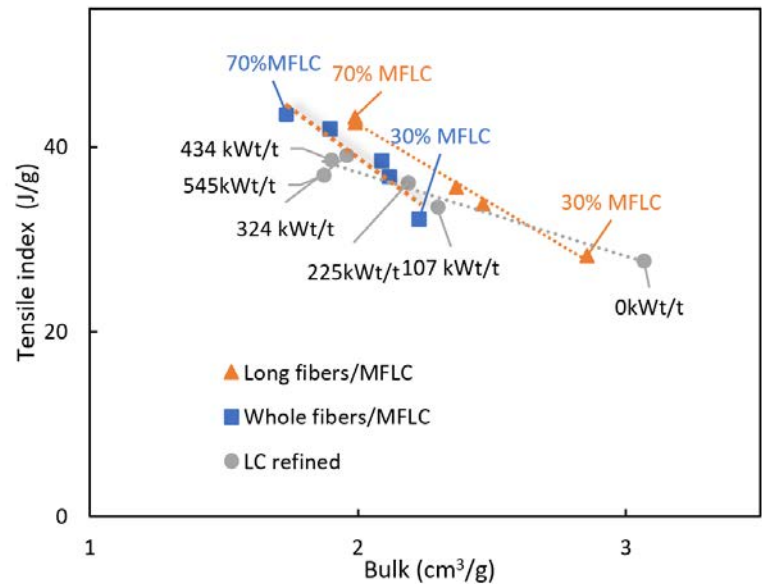


**Figure 1.** Relationship between tensile index and bulk for different composites.

Figure. 2 demonstrates that increasing the MFLC percentage from 30% to 70% decreased the tear index of all the composite sheets, with the lowest tear index observed at 70% MFLC. Additionally, composites made from long fibres and MFLC exhibited a higher tear index compared to those made from whole pulp and MFLC. A reduction in tear strength with increasing microfibril content has also been reported in other studies (Eriksen et al. 2008; Petroudy et al. 2014). We hypothesize that at high MFLC percentages, the microfibril network becomes strong enough that the long fibres no longer pull out but instead break, leading to a decrease in tear strength as the percentage of long fibres in the composites decreases. The composite sheets exhibited a higher tear index compared to the LC-refined sheets, primarily due to fibre shortening during the refining. In addition, despite the higher replacement of long fibres and whole pulp with MFLC in the composite sheets, the overall average fibre length remained longer than those produced from LC-refined, resulting in bulky structures and a higher tear index. The mean fibre length for long fibre fractions and whole pulp was about 2.8 mm and 1.5 mm, respectively while for LC-refined pulp, the mean fibre length was 1.2 mm at 107 kW/t, which dropped to 0.4 mm at 545 kW/t.

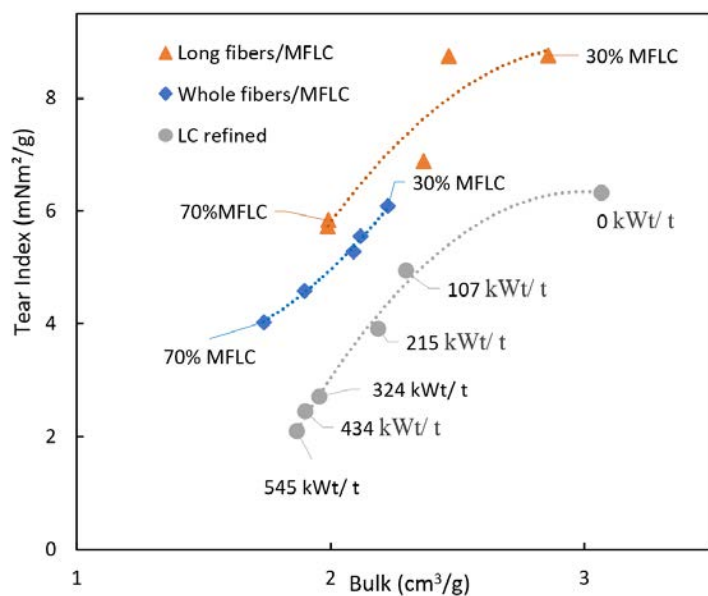


Figure 2. Relationship between tear index and bulk for different composites.

## Summary and Conclusions

This study explored the preparation of high-bulk, strengthened composite sheets for packaging by incorporating MFLC into SPF whole pulp and long fibres. We conducted a comparative analysis of the properties of the composite sheets with the sheets produced from LC-refined pulp. Initially, the effects of adding 0–20% MFLC were examined, and in this study, we extended MFLC content up to 70%. The results showed that increased refining energy in LC refining produced denser structures with high tensile strength but led to fibre shortening and tear strength, which may limit suitability for packaging. Adding up to 20% MFLC enhanced the tensile index and tear index of the composite sheets, with minimal impact on the bulk, highlighting their potential suitability for packaging. Higher MFLC levels (30–70%) further enhanced tensile properties but reduced the tear index. We conclude that moderate MFLC content is beneficial for applications requiring both strength and tear resistance, while higher MFLC levels (30–70%) can be advantageous for applications prioritizing tensile properties, with some compromise on tear resistance. These findings underscore the advantages of incorporating MFLC into SPF fibres to enhance specific properties relevant to packaging requirements.

## Future Work

We are exploring the development and characterization of MFLC film materials that may have applications to a wide variety of packaging applications.

## References

1. Areej F, Ashadie KM, Zakiah S, Ainun ZMA (2023) Pulping process for nonwoody plants. In: Pulping and papermaking of nonwood plant fibers. Elsevier, pp 17–32
2. Bajpai P (2018a) Chapter 12 - Pulping Fundamentals. In: Bajpai P (ed) Biermann's Handbook of Pulp and Paper (Third Edition), Third Edition. Elsevier, pp 295–351
3. Bajpai P (2018b) Biermann's Handbook of Pulp and Paper: Volume 1: Raw Material and Pulp Making. Elsevier
4. Bharimalla AK, Deshmukh SP, Patil PG, Nadanathangam V (2017) Micro/nano-fibrillated cellulose from cotton linters as strength additive in unbleached kraft paper: Experimental, semi-empirical, and mechanistic studies. *BioResources* 12:5682–5696
5. Brodin FW, Eriksen Ø (2015) Preparation of individualised lignocellulose microfibrils based on thermomechanical pulp and their effect on paper properties. *Nordic Pulp & Paper Research Journal* 30:443–451
6. Elahimehr A, Olson JA, Martinez DM (2015) Low consistency refining of mechanical pulp: how plate pattern and refiner operating conditions change the final properties of pulp. *Nordic Pulp & Paper Research Journal* 30:609–616
7. Eriksen Ø, Syverud K, Gregersen Ø (2008) The use of microfibrillated cellulose produced from kraft pulp as strength enhancer in TMP paper. *Nordic Pulp & Paper Research Journal* 23:299–304
8. Fernandez FJ, Martinez DM, Olson JA (2018) Investigation of low consistency reject refining of mechanical pulp for energy savings. *Nordic Pulp & Paper Research Journal* 33:21–27
9. Hammar L-A, Salmen L, Sandberg C, Sundstrom L (2010) The effect of process conditions on pulp quality development in low consistency refining of mechanical pulp-TMP. *Appita: Technology, Innovation, Manufacturing, Environment* 63:377–380
10. Jahangir ES, Olson JA (2020) Low consistency refined lignocellulose microfibre: an MFC alternative for high bulk, tear and tensile mechanical pulp papers. *Cellulose* 27:2803–2816

# PROJECT 3.1

## CHEMICAL MODIFICATION AND ADVANCED CHARACTERIZATION OF FIBRES

Authors: Kudzanai Nyamayaro, Emily D. Cranston, D. Mark Martinez

### Background

In this project, our aim is to modulate the bulk and tensile properties of pulp fibres through chemical modification. The chemical and mechanical modification of pulp fibres is a potential route to increase the bulk of paper without reducing the mechanical properties. Project 3.1. aims to apply chemical modifications to obtain low-density paper (i.e., high bulk) while maintaining favourable mechanical properties using BCTMP. Currently, we have demonstrated that HPMC, a low-cost and renewably sourced cellulose derivative, can be applied as a surface modifier for mechanical pulps to simultaneously enhance bulk and tensile properties of paper.<sup>1</sup> HPMC adsorbs onto the fibre surface, increasing fibre-fibre interactions through polymer entanglement which increases the tensile properties. Additionally, HPMC increases bulk by preventing fibre collapse during drying.

We have demonstrated that different molecular weight HPMCs are just as effective in improving both the tensile properties and the bulk. A greater increase in tensile index was observed for lower molecular weight HPMC compared to higher molecular weight. The improvement was attributed to improved solubility of lower molecular weight HPMC, leading to higher adsorption of HPMC onto the pulp. Additionally, low loadings of 0.25% HPMC were shown to be sufficient to improve the properties of BCTMP, highlighting that lower quantities of HPMC can be used to improve bulk and tensile properties. Lastly, we have shown that the binding of HPMC to BCTMP is not disrupted by refining, demonstrating the effectiveness and robustness of using HPMC to enhance the properties of mechanical pulp.

### Results

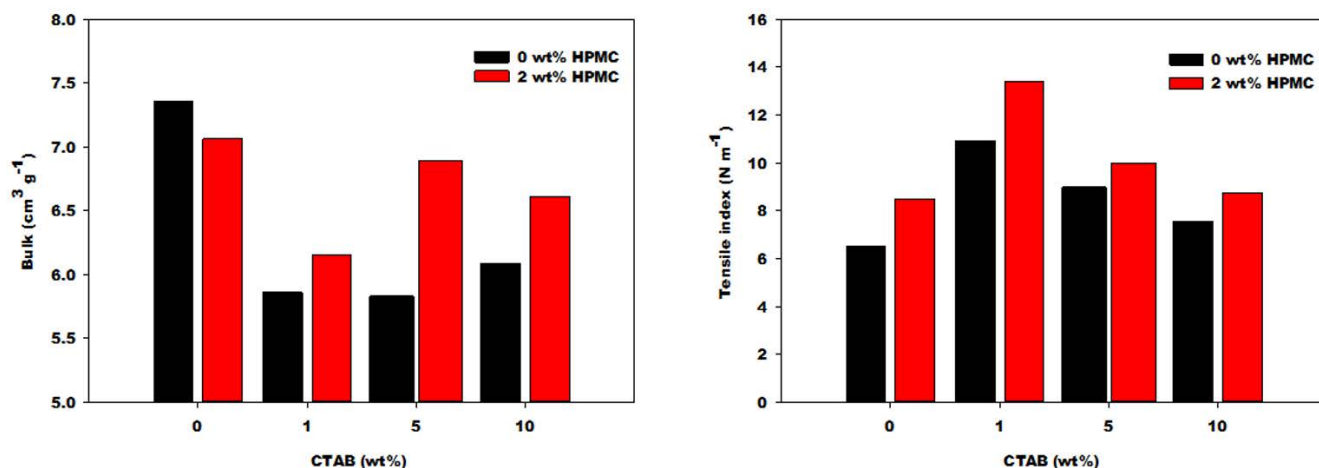
Since the last meeting, we have investigated whether the binding of HPMC is influenced by the presence of other additives. BCTMP handsheets were prepared using a pre-treatment method that involves adding HPMC and the additive (CTAB) into the pulp slurry prior to papermaking. In order to see the influence of the additives, the handsheets were not pressed. As shown in Figure 1, for BCTMP treated with CTAB, the bulk and the tensile properties were enhanced in the presence of HPMC. This confirms that the binding of HPMC and its improvement of the pulp properties is not influenced by the presence of other additives.

### Summary and Future Direction

In summary, the effectiveness and robustness of using HPMC to enhance the properties of mechanical pulp has been demonstrated. This is shown by preserving the improved properties in the presence of additives, with lower HPMC loadings, using HPMC with different structures, and through the refining process. Moving forward, the capability to apply this technology on a larger scale will be conducted by running pilot-scale trials.

### References

1. Ferreira, E. S.; Sugiharto, J. W.; Nyamayaro, K.; Martinez, D. M.; Cranston, E. D., Creating bulky papers with hydroxypropyl methylcellulose. *Cellulose* 2024, 31 (14), 8851-8862.



32

**Figure 1.** (Left) Bulk and (Right) tensile index of handsheets pre-treated with varying loadings of CTAB plus 2 wt. % of high molecular weight K100M-HPMC. Both bulk and tensile properties were enhanced by HPMC even in the presence of CTAB.

## ADVANCED CHARACTERIZATION THROUGH COMPUTED TOMOGRAPHY

Authors: Samuel Brown, Anderson Veiga, Mark Martinez

### Project 1. Liquid Absorption Project

#### Background

Enhancing or reducing liquid absorbency, a vital property in paper-based products, depends on accurately characterizing absorption behaviours. However, there is currently a lack of scientific consensus on these phenomena, particularly at the microscale. Classical models for flow in porous media, such as the Bell-Cameron-Lucas-Washburn (BCLW) equation, dictate that liquid should flow fastest in the largest pores of the system, following the relation  $\ell(t) \propto \sqrt{rt}$ , where  $\ell$  is the position of the wetting front,  $r$  is the capillary (pore) radius, and  $t$  is time. In paper, the largest pores are the inter-fibre pores (the spaces between the fibres). However, in studies of absorption in paper, there is general agreement that the fastest flow occurs along the fibres – some have observed this flow on the exterior wall surfaces<sup>1</sup>, while we previously observed axial penetration in the intra-fibre pores of the fibre walls<sup>2</sup>. It is important to reconcile these two observations, yet neither aligns with the

BCLW equation, as the fibres have a markedly smaller capillary radius (and larger viscous dissipation) than the inter-fibre pores. These observations of flow *on* or *in* the fibres suggest that such traditional models do not fully capture all the physical mechanisms required to describe absorption in paper accurately.

Although our former study using iron tracers confirmed that flow occurs in the intra-fibre pores of the fibre walls<sup>2</sup>, the static measurement methodology made it difficult to ascertain the dynamics of the absorption. Also, it did not present the opportunity to investigate the filling of the inter-fibre pores. Therefore, we devised new measurement techniques to investigate and quantify the absorption dynamics in paper, aiming to determine the specific pathway taken by liquid at the microscopic scale during imbibition and to clarify the microscale absorption behaviours leading to rapid absorption in the smaller pore system.

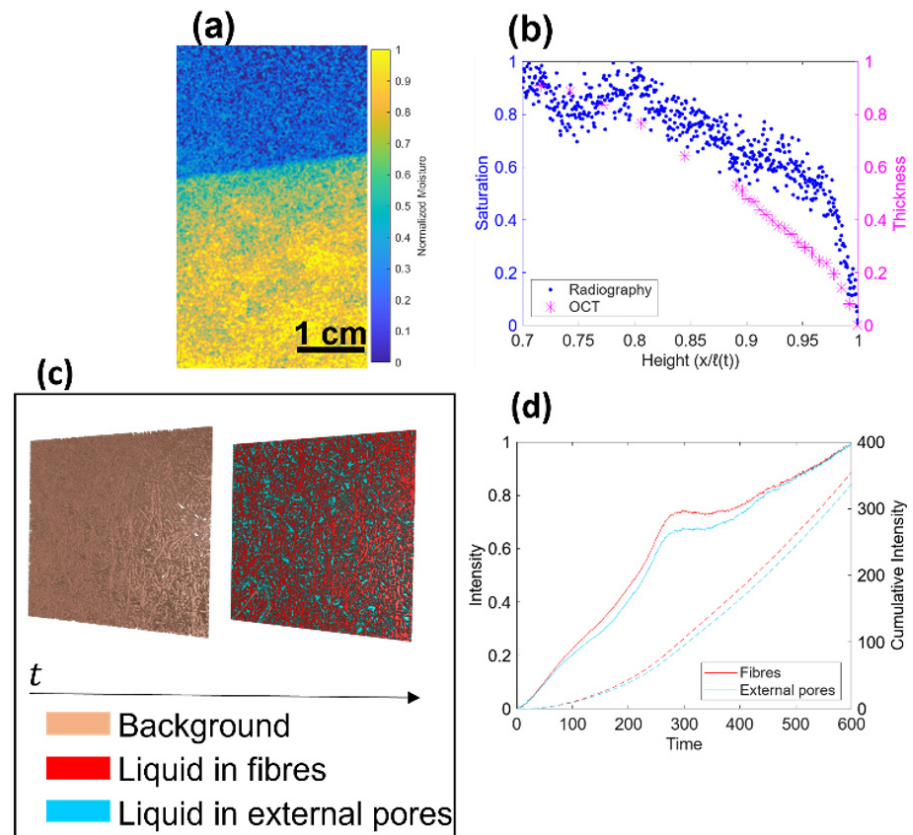


**Figure 1.** Overview of absorption results. At the macroscopic scale, an example radiograph is shown in panel (a) and the saturation and swelling profiles are shown in panel (b). At the microscopic scale, a dual-staining visualization is shown in panel (c), and a quantification of absorption rates is shown in panel (d).

# PROJECT 3.2

## Results

### *Macroscopic scale*

In the last reporting period, we detailed the development of new X-ray radiography and confocal microscopy techniques for measuring and visualizing the flow of liquids in paper. Since then, we have collected some evidence to identify the pathways taken by liquid during absorption. Shown in Figure 1 are the latest findings of the absorption study. At the macroscopic scale, we found the presence of a saturation gradient during absorption, evidenced by the X-ray radiograph shown in panel (a), where the paper is lightly saturated near the wetting front (teal colours) and highly saturated farther from the wetting front and closer to the reservoir (yellow colours). This observation can indicate the presence of two flow fields, but may also be explained by incomplete filling of pores. Therefore, we compare the saturation data from X-ray radiography to thickness data from optical coherence tomography (OCT) by scaling both datasets by the position of the wetting front  $\ell(t)$  in panel (b). Crucially, in this comparison, we note that saturation increases more rapidly than thickness near the wetting front – there is an increase in mass without an associated increase in volume. This observation confirmed the presence of two flow fields and motivated further microscopic study.

### *Microscopic scale*

We display the results from confocal microscopy experiments in panels (c) and (d) of Figure 1. In panel (c), we highlight the results from dual-fluorescent-staining of paper, used in conjunction with a new segmentation technique to separately visualize the flow through the fibres and external pores. Dual staining was performed by first applying Toluidine Blue O to the paper, rinsing the excess, and allowing the paper to dry. Images of the Toluidine-stained paper were captured in 3D using optical sectioning on the confocal microscope in the red channel. This background image was segmented, and each pixel was identified as belonging to either a fibre or an inter-fibre pore. Next, Fluorescein sodium was supplied to the paper, allowed to wick, and movies were captured in the green channel. In addition to enhanced visualization, this approach also provides the ability to quantify the filling rates of the fibres, such as shown in panel (d). Here it can be seen that liquid travels more quickly in the fibres compared to the external pores, aligning with the results from our prior study.

## Conclusions and Future Research

Combining our observations at the microscopic scale with results from our prior study using iron flow tracers<sup>2</sup>, we confirm that liquid penetration occurs axially through the intra-fibre pores in the fibre walls. However, it remains unclear why this is the case, as the fibres should have a much higher flow resistance than the inter-fibre pores due to their small size. It is possible that liquid is pumped from the external pores into the internal pores due to a pressure gradient, providing the additional driving force necessary to overcome the higher friction. To determine if this is indeed occurring, we have conducted experiments with altered samples that block certain absorption pathways and are developing a mathematical model to explain the results of these experiments.

We have also begun using the new imaging techniques to map the distribution of paper additives and assess their effects. The dual-staining technique was previously used to visualize the distribution of the HPMC treatment from Project 3.1, as discussed in the June 2024 newsletter, and will now be applied to investigate the effect of novel hydrophobic treatments.

# PROJECT 3.2

## Project 2. Labelling pulp fibres for X-ray tomography visualization

In previous reports, we presented a protocol for labelling long fibres in BCTMP handsheets using iron oxide nanoparticles (NPs). Segmentation was performed using either an advanced machine learning algorithm for samples scanned in air or the Max Entropy algorithm for samples scanned in oil. The iron-labelling protocol achieved high iron loadings (up to 16 wt.%) after a four-cycles, which significantly impacted the tensile properties of handsheets containing 2 wt.% or more labelled fibres. Current progress focuses on optimizing the labelling protocol to tailor the deposition of iron oxide NPs onto pulp fibres. Additionally, we aim to mitigate the adverse effects of the labelling agent on the tensile properties of handsheets with higher loadings of labelled fibres. Our ultimate goal is to use X-ray tomography to investigate the fibre network in pulp blends, such as BCTMP blended with NBSK.

### Results and Future Research

We employed a design-of-experiments approach to optimize the deposition of iron oxide NPs onto pulp fibres. By incorporating Fe (III) and Fe (II) salts, we increased the iron loading from the previously reported 4.5 wt.% to 9.6 wt.%. We also significantly reduced the protocol duration from nearly one week to approximately three hours. Current work compares the efficiency of the optimized protocol across various pulp fractions, ranging from long fibres to fines, and different types of pulp fibres, including BCTMP SPF, BCTMP Aspen, and NBSK. Our goal is to

develop a labelling protocol tailored to the surface charge content for each type of pulp fibre or size fraction, while preserving the characteristics of the original pulp fibres and reduce the impact on the mechanical properties of handsheets.

To address the adverse impact on tensile properties reported previously and restore a cellulose-like surface, we are developing a method to deposit cello-oligosaccharides onto labelled fibres. This innovative protocol involves producing cello-oligosaccharides and tailoring their deposition onto the fibre surfaces. Preliminary results indicate that the cello-oligosaccharide treatment promotes fibril growth on the fibre surface and forms a coating with properties resembling cellulose. However, further evaluation is required to confirm that this treatment restores the tensile properties of the labelled fibres, ensuring they behave similarly to unlabelled fibres.

### Acknowledgements

We thank Mr. Axel Drotz from the KTH Royal Institute of Technology for his contributions to the liquid absorption project while visiting over the summer to work on his Master's thesis.

### References

1. Bump, S. et al. Spatial, spectral, radiometric, and temporal analysis of polymer-modified paper substrates using fluorescence microscopy. *Cellulose* 22, 73–88 (2015).
2. Ferreira, E. S. et al. Mapping absorbency in cellulosic fibres with iron tracers. *Carbohydr. Polym.* 311, 120785 (2023).

# ERMP PHASE 3 TEAM



Nilgun Abali - WL student



Matthias Aigner - PDF UVic



Sneha Balaji - Mitacs student



Rodger Beatson - Professor BCI



Michael Bilek - Research Tech



Samuel Brown - PhD student



Yankai Cao - Professor CHBE



Jingqian Chen - PDF UBC



Siwei Chen - MASC



Thomas Clarito - COOP student



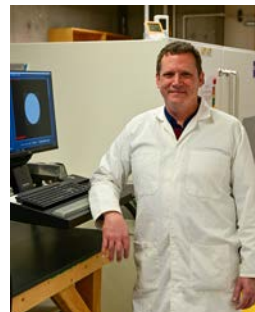
Emily Cranston - Professor CHBE



Hamza Dastgir, COOP student



Salman Dajani - COOP student



James Drummond - Microscopist



Mengqi Fang - PDF UBC



Elisa Ferreira - PDF UBC



Matheus Ferreira - WL student



Mariana Frias - PhD student



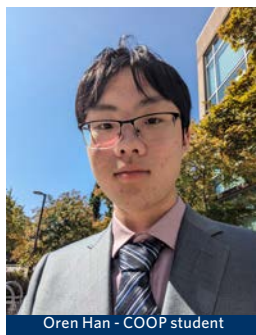
Samira Gharekhani - PDF UBC



Bhushan Gopaluni - Professor CHBE



Siddharth Groove - COOP student



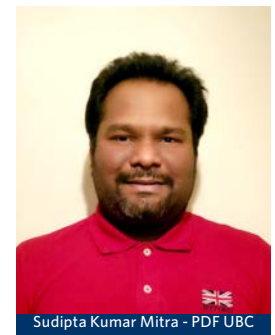
Oren Han - COOP student



Ryan Hlina - COOP student



Pierre Kasangana - PDF UBC



Sudipta Kumar Mitra - PDF UBC

# THANKS TO ALL OF YOU



Vijay Kumar Pediredla - PDF UBC



Amy Lai - COOP stud



Stephen Lee - COOP student



Juliana Lima - PhD student



Liyang Liu - PDF UBC



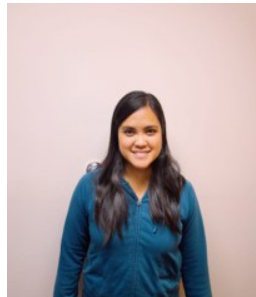
Kasish Mahajan - COOP student



Lewis Mason - MASC student



Mark Martinez - Professor CHBE



Claire Maulit - MASC student



Dua Naqvi - COOP student



Gloria Noki - MASC student



Kudzanai Nyamayaro - PDF UBC



James Olson - Professor MECH



Dev Parekh - Mitacs student



André Phillion - Professor McMaster



Renz Po - COOP student



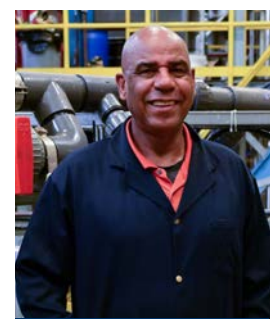
Shriya Rambhia - Mitacs student



Scott Rennecker - Professor Wood Science



Santiago Reynoso - Mitacs student



Norman Roberts - Research Tech



Kam Russell - COOP student



Farah Sadek - COOP student



Rasmita Sahoo - PDF UBC



Laurel Schafer - Professor CHEM



Reanna Seifert - Research Tech

# ERMP PHASE 3 TEAM



Noorpreet Sekhon - WL student



Priyanshi Shrivastava - Mitacs student



Aurélien Sibellas, PDF



Boris Stoeber - Professor MECH



Jason Sugiharto - COOP student



Nicole Ting - COOP student



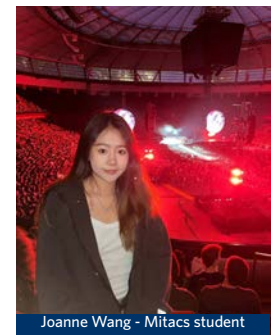
Heather Trajano - Professor CHBE



Daniela Vargas Figueroa - Manager



Anderson de Veiga - PhD student



Joanne Wang - Mitacs student



Yimin Wang - COOP student



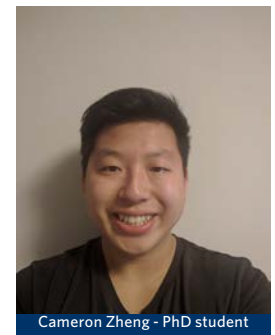
Peter Wild - Professor UVic



Adam Wu - PDF UBC



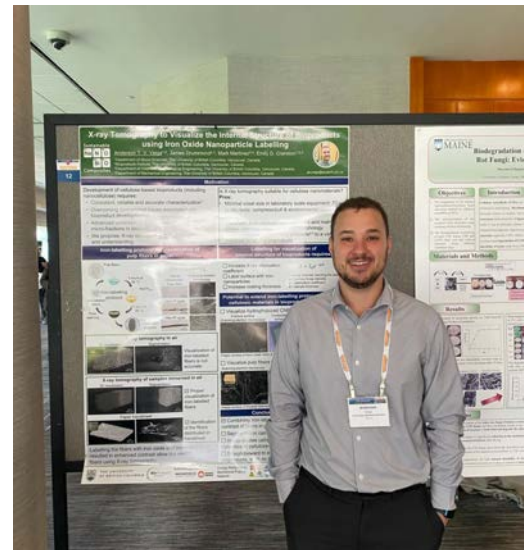
Fariba Yenaneh - PDF UBC



Cameron Zheng - PhD student

Page 39 (right): The ERMP team participated in several key conferences. The top row features Sam, Mark, and Boris at the International Paper Physics Conference (IPPC) in Germany. Additionally, Sam had the opportunity to present his research at TU Graz in Austria. Anderson and Mariana attended the TAPPI Nano Conference in Atlanta, Georgia, as shown in the top right and second rows. Matthias, Mariana, Fariba, and Daniela also participated in the International Mechanical Pulping Conference (IMPC) in Sundsvall, Sweden. Matthias delivered an oral presentation, while Mariana and Fariba showcased their work in the poster sessions. The final photo captures the team during the 2022 Whistler PacWest Conference, held alongside our Steering Committee meeting.

# SHARING OUR RESEARCH



# CONTACTS

You are welcome to contact any of the faculty or staff:

Daniela Vargas Figueroa  
Program Manager, UBC  
604-827-2390  
Daniela.Figueroa@ubc.ca

Mark Martinez  
Professor, UBC  
604-822-8564  
Mark.Martinez@ubc.ca

James Olson  
Professor, UBC  
604-822-5705  
James.Olson@ubc.ca

Rodger Beatson  
Professor, BCIT  
604-432-8951  
Rodger\_Beatson@bcit.ca

Laurel Schafer  
Professor, UBC  
604-822-9264  
Schafer@chem.ubc.ca

Peter Wild  
Professor, UVic  
250-721-8901  
PWild@uvic.ca

Bhushan Gopaluni  
Professor, UBC  
604-827-5668  
Bhushan.Gopaluni@ubc.ca

Emily Cranston  
Professor, UBC  
604-827-0627  
Emily.Cranston@ubc.ca

Boris Stoeber  
Professor, UBC  
604-827-5907  
Boris.Stoeber@ubc.ca

Heather Trajano  
Associate Professor, UBC  
604-827-1823  
Heather.Trajano@ubc.ca

Yankai Cao  
Assistant Professor, UBC  
604-822-2693  
Yankai.Cao@ubc.ca

Scott Rennekar  
Professor, UBC  
604-827-0637  
Scott.Rennekar@ubc.ca

André Phillion  
Professor, McMaster  
905-525-9140 x24046  
Philliab@mcmaster.ca

Visit our website

[www.EnergyReduction.ppc.ubc.ca](http://www.EnergyReduction.ppc.ubc.ca)

## PARTNERSHIP IS OUR STRENGTH

The supporting partners of this research program are:

AB Enzymes, Alberta Newsprint Company, BC Hydro, BCIT, Canfor, FPInnovations, Holmen Paper, McMaster University, Millar Western, NSERC, Paper Excellence, The University of British Columbia Pulp and Paper Centre, The University of Victoria, West Fraser and Valmet.

